University of Stavanger

Faculty of Science and Technology

MASTER'S THESIS

Study program: Master of Science in Petroleum Engineering Specialization: Natural Gas	Spring semester, 2021 Open access

Author: Ibrahim Seyidov

Programme coordinator: Zhixin Yu Internal Supervisor: Prof. Zhixin Yu External Supervisor: Tor Christensen

Title of master's thesis: **CO₂ capture by adsorption**

Credits (ECTS): 30

Keywords: CO₂ capture Direct air capture Adsorption Desorption Breakthrough Zeolites	Number of pages: 86 Stavanger, 14/06/2021

Acknowledgments

Abstract

The increasing concentration of CO_2 in the atmosphere entails casualties, mainly global warming issues. For quite a long time, considerable efforts have been dedicated to suppressing this issue. Amongst the proposed solutions, direct air capture (DAC) is deemed to be one of the most promising technologies in the future for mitigating the challenges caused by carbon dioxide.

In this thesis project, CO_2 removal by the DAC method using a suitable adsorbent, namely, zeolite, is studied. Adsorption and desorption processes on the Z8 test plant are implemented by applying the temperature swing adsorption (TSA) principle.

The test facility Z8 at Greencap Solutions includes a packed adsorbent bed and advanced instrumentation and control systems. It contains three adsorption columns, two of which are for water removal before the carbon capture. For moisture removal from flowing air, silica gel desiccant is deployed.

The CO_2 capture process is done by the flowing air over a packed bed of zeolite beads. CO_2 initially gets captured at the bed inlet, and after the progression of the capture process, the zeolite beads near the packed bed inlet becomes saturated with CO_2, and CO_2 is captured further into the bed. Near the end of the capture process, CO_2 is detected at the outlet of the packed bed, initially at very low concentrations. The concentration augments with time, and this is called breakthrough, and the CO_2 concentration trends a breakthrough curve.

Based on the breakthrough curves, the adsorption rate was examined, the amount of captured CO_2 was calculated both till breakthrough and complete test. In addition, the pressure drop during the adsorption process was also investigated and compared with the Ergun equation to have a better realization. It was found that a higher flowrate caused a faster breakthrough. Regarding the adsorption capacity, small size showed the highest capacity due to more active sites on the surface. However, as the adsorbent particle size declined, it caused more pressure drop due to the fewer void fractions.

Eventually, considering the obtained results from the experiments, a conclusion is made, and further work for improving the test plant is suggested.

TABLE OF CONTENTS

List of Figures

List of Tables

Nomenclature

Abbreviations

CCS   Carbon capture and sequestration

DAC   Direct air capture

DACCS   Direct air capture carbon sequestration

PSA   Pressure swing adsorption

TSA   Temperature swing adsorption

MEA   Monoethanolamine

IGCC   Integrated coal gasification combined cycle

ASU   Air separation unit

WGS   Water gas shift

MOF   Metal-organic framework

ZIF   Zeolitic imidazolate framework

AC   Activated Carbon

CBM   Carbon-based materials

PLC   Programmable logic controller

PFD   Process flow diagram

P&ID   Piping and instrumentation diagram

1. Introduction

Increasing CO_2 concentration in the atmosphere has become one of the vital concerns to our environment. CO_2 is a primary greenhouse gas which is one of the main reasons for global warming. Many measurements are taken globally to diminish the effect of greenhouse gases on our setting. The greenhouse effect is a natural process that warms the earth's surface by trapping the heat. When solar energy reaches the earth's atmosphere, some of this energy is reflected to space. In contrast, the others are absorbed and picked by the greenhouse gases and reradiated again to the earth, which will ultimately cause an increase in the earth's temperature. Among other greenhouse gases, CO_2 emissions are the major, representing 76% of the emissions to the atmosphere [1].

It is an observable fact that global warming is a threatening concern for the environment, and carbon capture and sequestration (CCS) emerges as a viable option for alleviation purposes. Oxy-fuel, pre-combustion, and post-combustion are the leading technologies for carbon capture and thus mitigation of global warming. Aside from these methods, CO_2 can be captured directly from the air, called direct air capture.

1.1 Objective

The main objective of this thesis is to study the direct air capture process and observe the difference in the capture process by modifying the superficial air velocity and adsorbent size.

Different tasks of the project can be specified as follows:

1) To get familiar with the Z8 test plant designed by Greencap Solution
2) To study the effect of adsorbent size for CO_2 capture
3) To analyze the essence of superficial air velocity for the capture process
4) To define the amount of CO_2 captured at breakthrough and after the complete test
5) To assess and discuss capture rates based on the shape of breakthrough curves
6) To evaluate the pressure drops over the packed bed
7) To discuss the improvements needed for the test plant

1.2 Outline of Thesis

The thesis is experimental and studies the direct air capture on the Z8 plant designed by Greencap Solutions and its applicability in large-scale industrial applications.

The theoretical background of this project is reviewed in Chapter 2. A more detailed explanation of the test plant is described in Chapter 3, including the process flow sheet files of both adsorption and desorption processes. Furthermore, the tools and instruments deployed for the data logging can also be found in Chapter 3.

Chapter 4 covers the results and discussion part acquired during the experiments. The breakthrough curves plotted, capture rates and pressure drop over the packed bed discussed, and eventually captured CO_2 amount calculated.

In Chapter 5, the conclusion and further work are addressed.

2. Literature Survey

2.1 CO_2 and greenhouse effect

CO_2 can be encountered naturally in the atmosphere as a trace gas. CO_2 can be entrapped in the atmosphere by human activities such as scorching fossil fuels, biological materials, solid waste, and so on. CO_2 is the main greenhouse gas that entails global warming. Humans have unequivocally brought about the tremendous rise of CO_2 content in the atmosphere (by 35%) since the industrial revolution started. As a side effect, the increment in global average temperature and sea level has become a striking trepidation. However, despite its dire consequences like global warming issues, CO_2 has copious superiorities for humankind. The foremost positive role of CO_2 is being the primary fount for the photosynthesis process [2] [3] [4].

As a matter of fact, the atmosphere is composed of 78% nitrogen, 21% oxygen, and 1% of other gases. CO_2 presence in the atmosphere is about 400 parts per million (ppm); in other words, 0.04 vol. %. For the past ten thousand years, the CO_2 content in the Earth's atmosphere was stable at roughly 280 ppm. However, from the mid-18th century, the scenario began to swap with the increase of CO_2 amount in the atmosphere as in Figures 2.1 and 2.2 below:
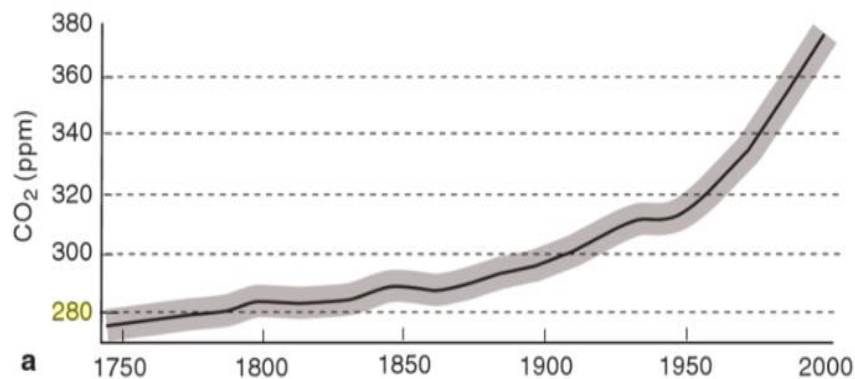
Figure 2.1: Atmospheric CO_2 content analysis based on ice core record from 1750 to 2000 [2]
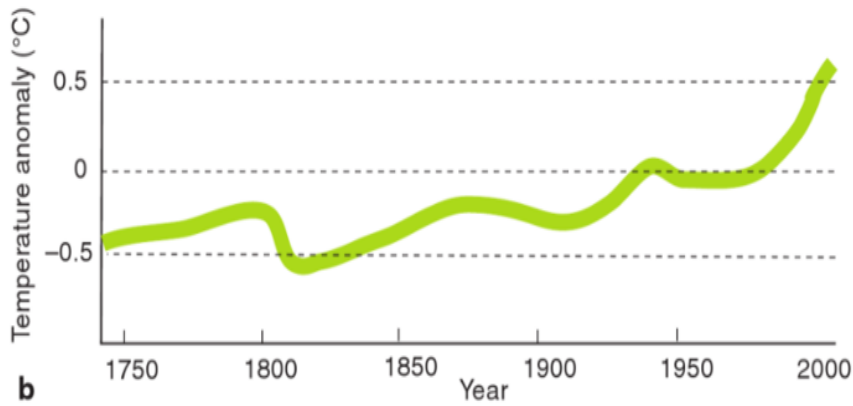
Figure 2.2: Northern hemisphere temperature record from 1750 to 2000 [2]

As shown in Figure 2.1 above, a sharp rise embarked on around in the 1940s, and by 1950 the increment level reached around 310ppm. This concentration was the highest in the past two million years [2].

Regarding the sea level, it has also created vast anxiety across the world, being risen by approximately 8 inches over the past 100 years. The main incentive for it is the global warming caused by greenhouse gases. The temperature increase triggers the melting of glaciers and ice sheets and eventually getting shrunk. According to the obtained satellite data, sea level commenced elevating nearly twice the rate seen over the past century, as shown in Figure 2.3 [4].

Figure 2.3: The cumulative decline in glacier ice from 1960 to 2000 [4]

2.1.1 CO_2 physical properties

At standard temperature and pressure, CO_2 is an odorless, colorless, and non-flammable gas, and its density is nearly 1.53 times that of air, namely, 1.98 kg/m^3. However, at high concentrations, it can give a severe, acidic smell.

At pressure less than 520 kPa, CO_2 has no liquid phase. At a 1atm pressure, temperatures below -78.5 °C, gas converts to solid-state and called dry ice. Liquid CO_2 can be configured at pressures above 520 kPa. The triple point is around 520 kPa at 217 K, and the critical point is at 7.39 MPa at 31.03 °C, respectively.

Another amorphous glass-like solid form of CO_2 is called carbonia and is only encountered at high-pressure conditions [5]. The main physical properties can be reflected in Table 2.1 below [6].

Molecular weight (g/mol)	44.01
Critical temperature (°C)	31.1
Critical pressure (bar)	73.9 bar
Boiling point @ 1.013bar (°C)	-78.5
Specific volume @ STP	0.506m^{3}kg^{-1}
Gas density @ STP	1.976 kg m^{-3}
Viscosity @ STP	13.72 μN.s m^{-2}
PH of saturated CO_2 solutions	3.7

Table 2.1: Physical properties of CO_2 [6]

To conclude, CO_2 physical properties are highly dependent on temperature and pressure and can vary based on changes in these two parameters. Figure 2.4 below shows this relationship in a visible way [6].
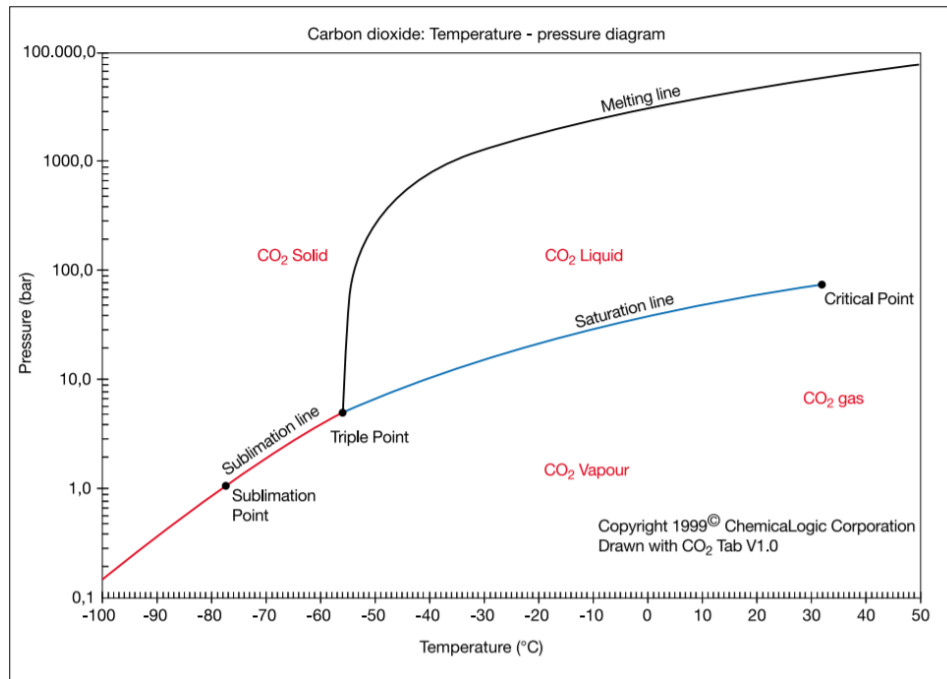
Figure 2.4: Phase diagram of CO_2 [6]

2.1.2 CO_2 chemical properties

At standard temperature conditions, gaseous CO_2 is not considered to be very reactive. The CO_2 molecule is stable and needs much effort to be decomposed into simpler compounds. Nonetheless, through excessive temperature or ultraviolet light, it can be broken down.

$$CO_2 \rightleftharpoons CO + 0.5O_2 \tag{2.1}$$

Generally, reactions happening between CO_2 and other substances are influenced just at high temperatures or by virtue of catalysts. Reduction of CO_2 to CO ensues by getting into reaction with hydrogen, namely, the reverse of the Water-gas-shift (WGS).

$$CO_2 + H_2 \rightleftharpoons CO + H_2O \tag{2.2}$$

Moreover, carbon monoxide can also be formed by the reaction of CO_2 with C at high temperatures:

$$CO_2 + C \rightleftharpoons 2CO \tag{2.3}$$
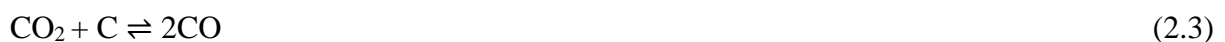
At elevated temperatures, using metals such as Ni or Co, the reduction of CO_2 to carbon is also plausible. Miscellaneous reactions with CO_2 have a colossal commercial necessity.

6

For instance, the reaction of ammonia with CO_2 creates ammonium carbamate. When it is dehydrated, it yields urea, a very substantial compound, mainly as a fertilizer.

$$CO_2 + 2NH_3 \rightarrow NH_2COONH_4 \tag{2.4}$$

$$NH_2COONH_4 \rightarrow NH_2CONH_2 + H_2O \tag{2.5}$$

The released H_2O can amalgamate with carbamate to generate ammonium carbonate or ammonium hydrogen carbonate as below [5]:

$$NH_2COONH_4 + H_2O \rightarrow (NH_4)_2CO_3 \tag{2.6}$$

$$(NH_4)_2CO_3 \rightarrow NH_4HCO_3 + NH_3 \tag{2.7}$$

2.2 Adsorption process

Adsorption is considered a surface phenomenon, where ions or molecules, atoms from gas, liquid, and dissolved solid adhere onto the surfaces. The adsorption process of CO_2 is implemented by the specific adsorbent materials, which are characterized as highly selective materials towards CO_2 uptake. The description of the adsorption process is most frequently identified through isotherms.

Physical adsorption and chemical adsorption are subcategories of the adsorption process. In physisorption, the process arises by the interaction of intermolecular forces, namely, Van der Waals forces. Low-temperature operation conditions, fast adsorption rate, low adsorption heat are the major characterizations of physical adsorption. In physisorption, as the intermolecular attraction is not strong, the general structure of the adsorbate barely gets modified, and the capability for regeneration of sorbent materials is very high.

Chemical adsorption involves the exchange and transfer of valence electrons between molecules and molecule adsorbents on the surface of adsorbent materials. In other words, the chemisorption process is based on the formation and destruction of chemical bonds. In contrast to physisorption, the adsorbed substance cannot be separated readily and is often supposed as irreversible [7] [8].

The physisorption and chemisorption processes can be schematically illustrated in figure 2.5.
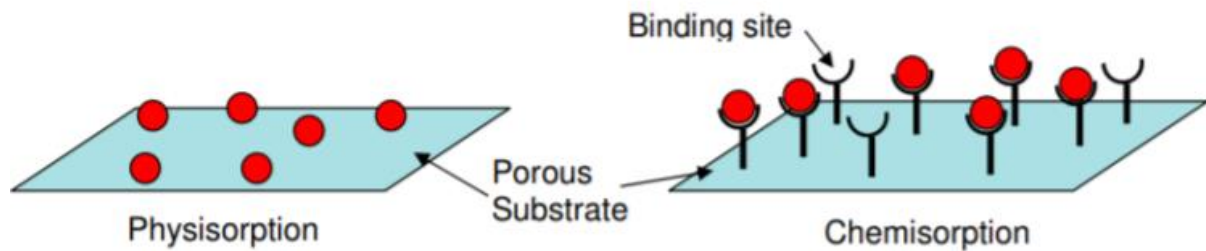
Figure 2.5: A superficial overview of physisorption and chemisorption phenomenon bonding[8].

Table 2.2 below underlines the main differences between physisorption and chemisorption:

| | Adsorption categories | |
	Physical adsorption	Chemical adsorption
Adsorption force	Van der Waals force	Chemical bond force
Selectivity	Nonselective adsorption	Selective adsorption
Adsorption layer	Single or multiple layers	Single-layer
Adsorption heat	Low	High
Adsorption rate	Fast	Slow
Stability	Instable	Stable

Table 2.2: Overview of the physical and chemical adsorption [7]

2.2.1 Pressure Swing Adsorption (PSA)

The working principle of the PSA process is based on the principle that, under high pressure, gases are more prone to be attracted (adsorbed) to solid surfaces. The reverse process is relevant for desorption. When the process swings to lower pressure, it tends to desorb the adsorbed material. By this, the separation of gas mixtures becomes plausible.

Depending on the number of adsorbers, PSA can be classified into single-bed and multi-bed processes. Generally, PSA operation includes pressurization of inlet gas, adsorption at high pressure, depressurization to atmospheric pressure, and CO_2 liberation.

Figure 2.6 below elucidates the PSA process of the single-bed category:
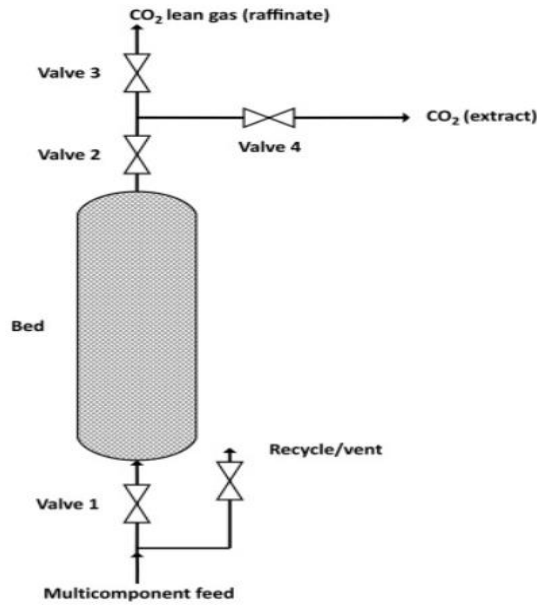
Figure 2.6: Single-bed PSA process [9]

At first, valve 4 is shut, and valves 1, 2, and 3 are opened. Apparently, because of the entrance of the gas feed containing CO_2, the pressure of the bed grows further until the P_2 (elevated) pressure level, and whereby the column becomes saturated with CO_2 (CO_2 adsorbed). Through adsorption and pressurization, CO_2 is recovered in the raffinate flow. Afterward, to depressurize the column down to the initial P_1 level, valve 4 is opened, whereas valves 1 and 3 are latched. After the acquisition of the P_1 pressure, valves 2,3, and 4 are closed, and valve 1 is opened. In this case, the stream is halted or led to another place for the redundant CO_2 extraction purpose. Subsequently, The column is cleaned with a part of lean carbon dioxide gas captured by valves 2 and 3. The separated CO_2 can be recycled to the storage tank or expelled into the atmosphere (not recommended) [9].

2.2.2 Temperature Swing Adsorption (TSA)

TSA is another method that is widely utilized for CO_2 separation from gas streams. The technique is similar to PSA, but, instead of pressure, the temperature is cycled. TSA relies on the principle that the higher the temperature, the less adsorption of CO_2 will be observed. Because of that, during the desorption process, the temperature is always increased for better efficiency. It is also important to accentuate that alongside the temperature change, the passage of purge gas (or steam) is commonly ensured for sweeping the desorbed components.

Purging the bed creates conspicuous challenges, such as making the desorbed CO_2 more dilute. Consequently, numerous technological approaches have been debated to cope with this hardship [10] [11].

Modification of the purging gas (i.e., H_2O or CO_2 instead of N_2) or heating the sorbent indirectly by dint of heat exchangers could be better solutions. If so, by the use of heat exchangers, there will be no need for carrier gas for the regeneration of the sorbent. Therefore, captured CO_2 can be recovered without being faced with dilution difficulties [10].

Figure 2.7 shows one of the probable indirect heating followed by hot product gas purge regeneration cycles comprising of 4 steps: feed at low temperature (first step), regeneration by heating the bed(second), direct counter-current hot gas purge with CO_2 output recovery (third), and finally cooling stage (fourth step).
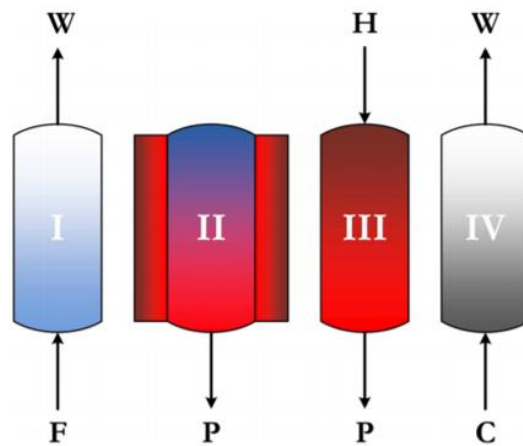
Figure 2.7: Cycle steps and their sequence. F=feed gas, W=waste gas, P=product gas (CO_2), H=hot purging gas, C=cooling N_2 gas [11].

First, from the bottom side, the feed gas enters the column at low temperature for CO_2 adsorption, and the process ends when CO_2 concentration constitutes 3% in the effluent. After the adsorption, the bed is exposed to a high temperature by the electric furnace under closed column valves. Then, the bottom valve is unfastened, and at the same time, a hot stream of product gas (as a purge gas) is fed from the top of the bed for desorbing the adsorbate. After the desorption process, the bed is cleaned and cooled by N_2. N_2 both purges and cleans the bed and makes it ready for further adsorption processes [11].

2.3 Carbon Capture and Sequestration

Carbon capture and sequestration (CCS) is a very vital tech to diminish CO_2 emissions from industrial sectors. There are various CCS techs that are dependent on the origin of CO_2 [12]. Post-combustion, pre-combustion, and oxyfuel are the leading technologies for carbon capture [13]. Furthermore, there is another method called Direct Air Capture, where the carbon-catching process is fulfilled directly from the air [12].

Since natural climate solutions are not satisfactory enough to alleviate climate changes, CCS is in the hub of interest zone. There is tremendous interest from the scientific community, the international political community, and the corporate world. Based on the specific considerations, it is aimed that by the end of the century, it will be needed to remove 640-950 billion tonne of CO_2 from the atmosphere in order to keep global temperatures stable at or below 1.5 °C above preindustrial temperatures [12].

The application of CCS in power plants is divided into 3 main stages. The first stage involves CO_2 separation from the power plant stream (CC), which is subsequently followed by the transportation of the captured CO_2. The final step is about the storage or sequestration of CO_2 into geological sites [13].

Figure 2.8 gives a detailed overview of carbon capture and storage procedures.
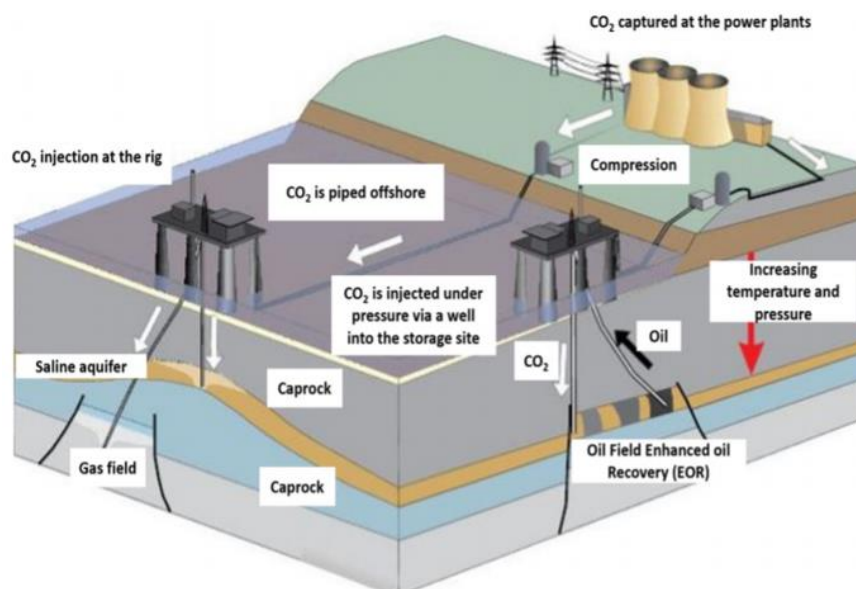
Figure 2.8: CO_2 capture and storage infrastructure using geological formation [13]

2.3.1 Post-combustion

As part of carbon capture and storage, post-combustion capture refers to the CO_2 separation from power plant flue gas prior to compression, transportation, and storage in geological formations. The purpose of the post-combustion capture technology is the removal of carbon dioxide from flue gases. In a typical coal-fired power generation system, fuel is burned with air in a boiler to produce steam, and the steam drives a turbine to generate electricity [14].

As the name suggests, carbon capture is performed after the combustion of the fuel. First, the high-temperature flue gas produced from the large-scale fossil fuel combustion process is cooled down to temperatures between 40 and 60 °C before being introduced to the absorber. In the absorber, the amine solvent (lean amine) is bonded with CO_2. On the top of the absorber column, exhaust gas is observed, which can be emitted directly to the atmosphere or used for various intents (e.g., industrial heating processes). As the gas elevates in the tower, liquid solvent is added from the top reacting with CO_2 in the flue gas.

After waiting for a certain time, CO_2 sinks into the column and leaves from the bottom of the tank. The amine rich in CO_2 is pre-heated in a heat exchanger before being transported to the stripper. The rich solution is then pumped to Stripper Tower, heated up to temperatures between 100 and 140 °C for the solvent regeneration purpose. Eventually, it causes the separation between the solvent and CO_2. The solvent can be recollected from the bottom of the column for being reused in the future. At the top of the stripper, a condenser plays a role in the recovery of steam left from the stripper and fed back to the desorber. Eventually, CO_2 is released from the top of the column and compressed for transportation. Figure 2.9 below illustrates the post-combustion process [13] [15].
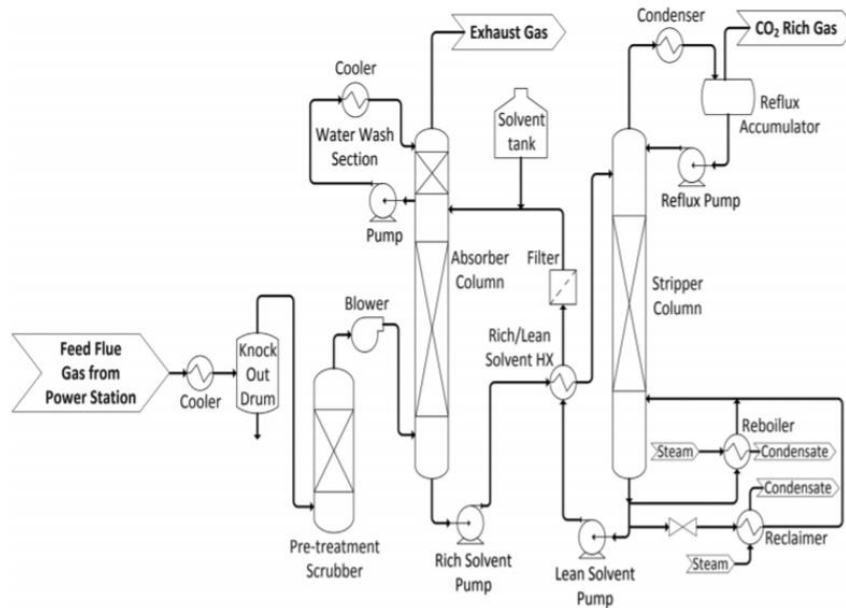
Figure 2.9: Post-combustion carbon capture process layout [13]

Post-combustion capture is assumed as the best tech available, especially for coal-fired power plants. At present, the technology functions based on solvent scrubbing (absorption) using amine solvents (mainly monoethanolamine (MEA)) [14]. There are myriad post-combustion gas separation and capture technologies that are constantly under investigation. Figure 2.10 shows absorption, adsorption, cryogenics, membranes, and biological separation technologies that can be harnessed with post-combustion capture [14].
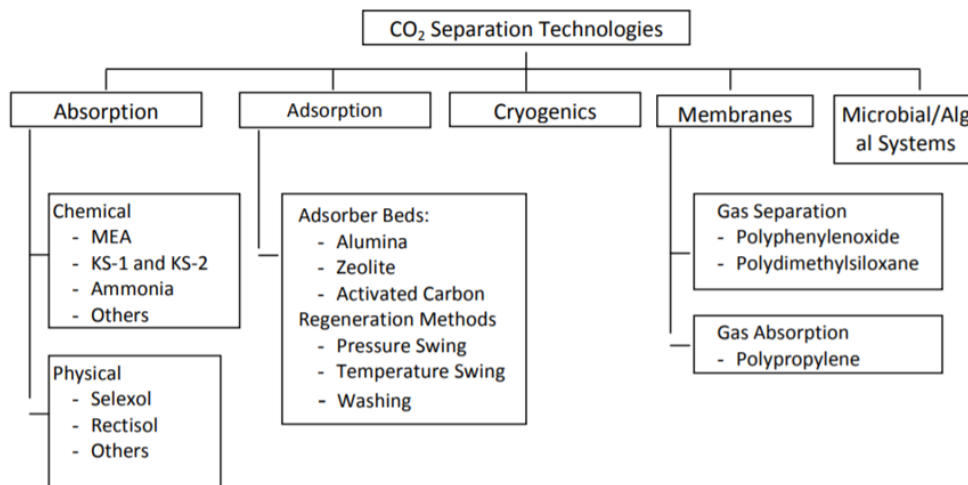
Figure 2.10: Process technologies for post-combustion CO_2 capture [16]

2.3.2 Pre-combustion

Pre-combustion capture is another method that concerns the treatment of syngas composed mainly of carbon monoxide and hydrogen. Pre-combustion is considered as a part of Integrated Coal Gasification Combined Cycle (IGCC) systems. In this method, CO_2 is removed from the fuel before combustion, in the absence of pollutants, like SO_x and NO_x. Physical absorption, membranes, and pressure-swing adsorption are the most auspicious techs for pre-combustion [17].

Initially, the air separation unit (ASU) separates air into its basic components, such as oxygen and nitrogen, and produces a stream of almost pure oxygen. Then, oxygen is injected into the gasifier together with fuel. The result of the gasification process is syngas. This syngas is then transported to Shift Reactor, where steam is added, and water-gas shift reaction (WGS) is implemented. In the shift reactor, CO is converted into CO_2 and H_2 [17].

$$CO + H_2O \leftrightarrow H_2 + CO_2 \tag{2.8}$$

Ultimately, the output is dispatched to desulphurization and CO_2 separation. CO_2 can be captured mainly by using the absorption method like in post-combustion. Eventually, CO_2 is then dehydrated, compressed, and ready for transportation, while hydrogen is deployed as input to various power generation applications.

Figure 2.11 highlights pre-combustion PFD for gasification power plant [18] [19].
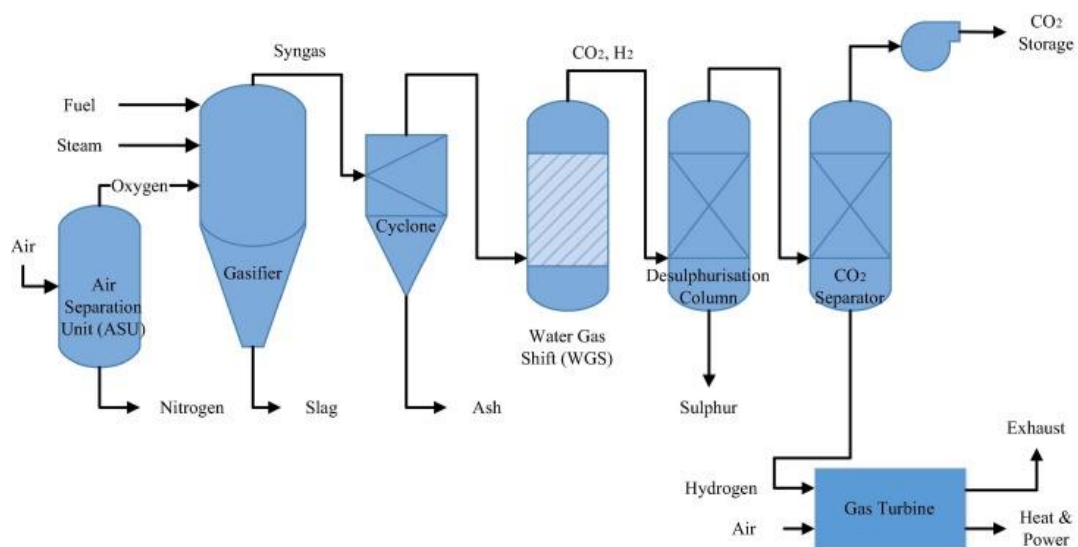
Figure 2.11: Pre-combustion process flow diagram for gasification power plant [19]

2.3.3 Oxyfuel

In oxyfuel combustion, fuel is burnt with almost pure oxygen ($> 95\%$) instead of air. It is commonly used in glass, metallurgical industries as well as thermal energy engineering. The liberation of nitrogen triggers a reduced energy demand for bringing the gas up to the correct combustion temperature.

In an air separation unit (ASU), oxygen is split up from other components of air. Almost pure oxygen is commingled with the recycled flue gas (from the boiler) prior to the combustion process taking place in the boiler. Blending the pure oxygen with a large proportion of recycled flue gas (2/3) is a very crucial part of the process to provide correct heat transfer characteristics. The mixture of oxygen and exhaust gas should be kept in such a balance that the pulverized coal oxy-combustion flame has alike heat transfer attribute to that of an ordinary air-fired system [20].

A generated heat by combustion can be used for different purposes, such as power generation. The fuel gas generated by the combustion consists of CO_2 and H_2O, which are circulated into the boiler to control the temperature. Eventually, in the condensation unit, CO_2 can be separated and compressed for transport. The main goal of deploying this technology is to generate a flue gas with high CO_2 concentration and H_2O vapor and afterward by applying low-temperature purification and dehydration processes to separate the CO_2 from the flue gas [21] [20]. Figure 2.12 represents the schematic diagram of the oxyfuel combustion process.
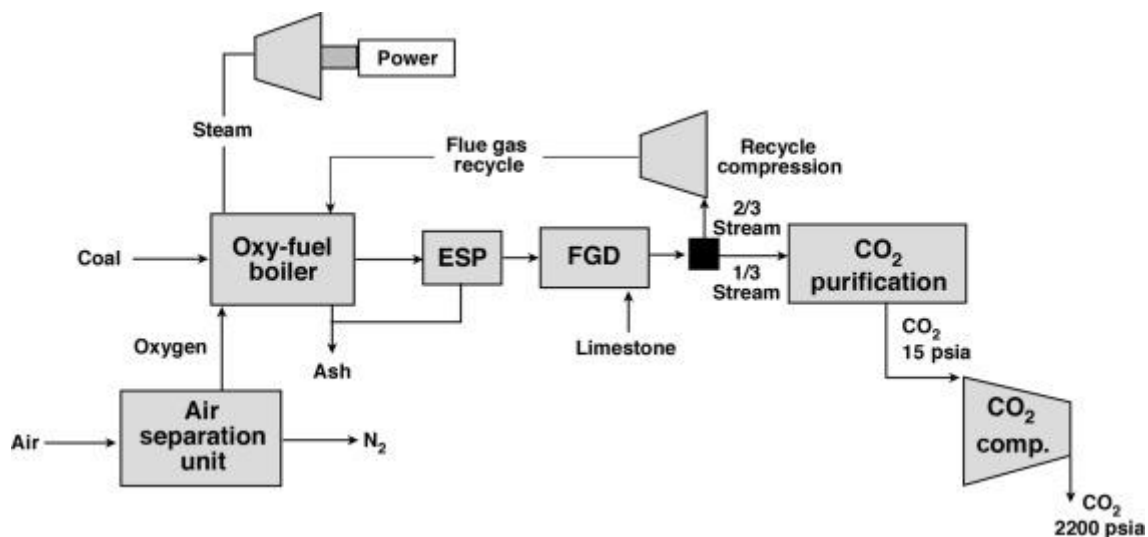
Figure 2.12: Schematic diagram of Oxyfuel combustion, ESP (electrostatic precipitator), FGD (Flue Gas Desulphurisation) [20].

In summary, the principal benefits of oxy-fuel combustion are high CO_2 purity, fewer NO_x emissions [21]. Furthermore, because of the lofty concentration of CO_2 in the exhaust gas, neither physical nor chemical sorbent is needed to liberate CO_2 [22].

2.4 Direct Air Carbon Capture (DAC)

DAC is an essential technology for mitigating global warming casualties by capturing CO_2 directly from the air. Every year by applying the DAC process and using chemicals known as sorbents, it becomes feasible to remove a significant quantity of CO_2 from the air. There are two main processes that sorbents mainly work. These are absorption and adsorption processes.

In the absorption process, CO_2 dissolves into the sorbent material, whereas in the adsorption process, CO_2 molecules adhere to the surface of the sorbent materials. In both methods, CO_2 should be capable of being released from sorbent materials for further sequestration or utilization purposes [23].

The first application of DAC was introduced in cryogenic air separation plants, which were then deployed in space stations and submarines. One of the main drawbacks of the first systems was that they were not regenerative [24].

Direct CO_2 capture from air generally consists of three main steps:

a) The ambient air is directed towards the given sorbent (i.e., absorption or adsorption), which is selective to remove the CO_2. The suction could be enhanced through fans to have sufficient contact area between the CO_2 and the sorbent (contacting)

b) Separation of the CO_2 from the ambient air and bounding to the absorbing or adsorbing material (aqueous-based solution or solid material (capturing)

c) Removal of the captured carbon dioxide from the sorbent material to regenerate the aqueous solution or solid material to re-use it again (regeneration)

Compared to other CO_2 capture technologies, DAC is not well-developed that can dwindle the significant amount of CO_2 concentration in the atmosphere. Nonetheless, DAC also seems to be a promising technology in the future, and therefore there are several pilot projects and miscellaneous research done on the improvement of DAC [25].

2.4.1 Technologies for CO_2 capture from air

In comparison to CO_2 in flue gases, it is overly dilute in the air, meaning that a high amount of energy is needed for its uptake from surrounding air. However, one of the primary considerations is that any action for CO_2 capture should flinch the utilization of a striking amount of energy on processing bulk air for CO_2 elimination [26].

DAC is implemented by dint of sorbents which can catch CO_2 under certain circumstances. So, in the presence of moisture and near to room temperature, the selected sorbent should have a high range of selectivity towards CO_2 and be very stable. In addition to that, it must be readily regenerative considering its on-site utilization intentions [26].

Sorbent materials can be both solids and liquids. Solid sorbents have myriad advantages, such as being less prone to lose volatiles, owning better kinetics, and therefore, most DAC processes utilize solid sorbents. Notwithstanding this, there are some exceptions made by numerous companies, such as by 'Carbon Engineering,' which uses hydroxide solution instead. Another exception is made by Custelcean and co-workers, where the CO_2 is captured from the air by aqueous-phase sorption followed by precipitation into a crystalline phase, with a subsequent release using concentrated solar power [26].

Causticization with alkali-earth hydroxides, carbonation, and organic-inorganic hybrid sorbents consisting of amines supported in porous adsorbents are other appropriate technologies offered for DAC. Aside from it, artificial trees are one of the cutting-edge DAC methods to suck up more CO_2 from the air than natural trees. CO_2 is surmised to be captured in a filter, removed, and stored in this method.

Another method is the one that deploys a polymer-based ion exchange resin and is valid only at a temperature of 40 °C. Because of the changes in humidity, it entails the apace release of the CO_2 captured from the air rather than using a kiln which results in less energy demand and a financially practical manner [25].

In all circumstances, heat and electricity input required for the operation of direct air capture and carbon sequestration (DACCS) must preferentially originate from low-carbon sources. According to one analysis, if the electricity needed for the DACCS plant is generated from the gas power plant (without CCS), from gas combustion, one would get back about 70–90% of that captured CO_2 by the DACCS plant [23].

2.4.2 DAC by absorption using liquid solvents

This method relies on the absorption process of CO_2 onto solvents. For the inception of the process, the air is dispatched toward the absorbent material, where CO_2 is absorbed by the based solution (NaOH or KOH).

Air contactors and regeneration facilities are considered major parts of a liquid solvent direct air capture system. In Figure 2.14, an aqueous KOH (potassium hydroxide) solution goes into reaction with the CO_2 grasped from the air and creates water and K_2CO_3 (potassium carbonate) in an air contactor. Afterward, K_2CO_3 is dispatched to a causticizer, where it reacts with calcium hydroxide ($Ca(OH)_2$) and converts to $CaCO_3$ (calcium carbonate) precipitate. Then, $CaCO_3$ slurry is transported to clarificatory and filter press to get rid of water. Subsequently, after the liberation of water, it is fed to a calciner. In an oxy-fired kiln, $CaCO_3$ precipitate is heated with natural gas (NG) up to around 900 °C. After the heat process, it disassociates into solid CaO and CO_2, which can be squeezed and sent to geological sites for long-term storage.

Eventually, in Slaker, CaO gets into reaction with H_2O exothermically to reform $Ca(OH)_2$, which is reused in the causticizer [27].

Figure 2.13 below elucidates the general process described above:
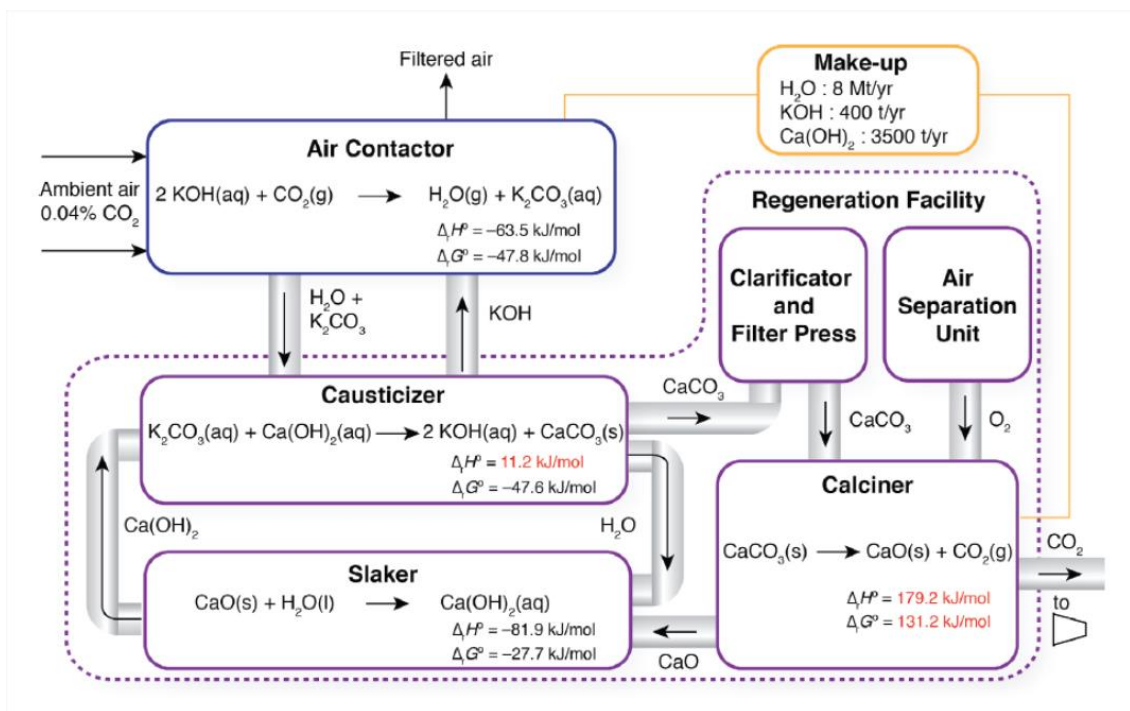
Figure 2.13: Simplified process flow diagram of a generic liquid solvent-based DAC system [27].

2.4.3 DAC with solid sorbent systems

The main discrepancy with liquid solvent systems is that instead of the absorption process, adsorption is applied. Solid sorbent DAC has two primary processes, namely, adsorption and desorption. In such a system, by dint of air suction and being blown through a solid adsorbent, CO_2 can be grabbed on the surface of solid adsorbent materials. After implementing the adsorption process, the desorption process is carried out to liberate CO_2 from the adsorbent and make it usable for further operations. In the last step, the solid sorbent is exposed to the cooling process before being introduced to further operations [27].

Figure 2.14 below illustrates a short overview of DAC with solid sorbent systems:
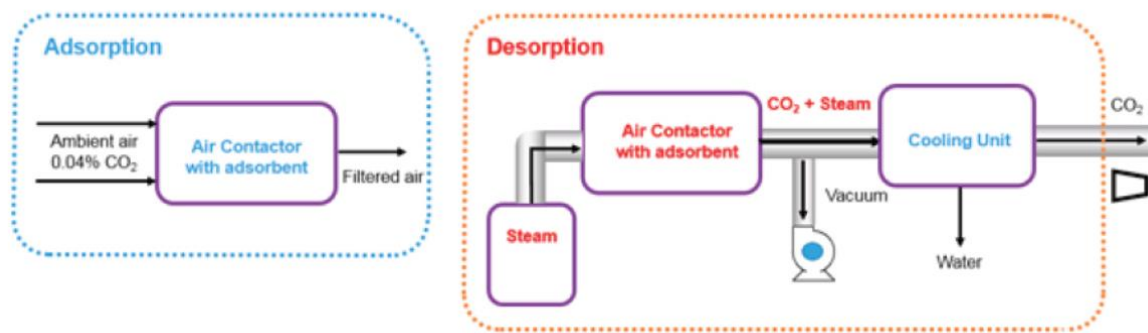
Figure 2.14: Schematic illustration of two-step, sorbent-based DAC process [27].

2.4.4 The thermodynamics of DAC

The extraction of CO_2 from the air demands a certain amount of energy. The main distinguishing side of DAC compared to other carbon capture technologies is that the CO_2 concentration in the air is unambiguously lower than that of the coal-fired power plant. (0.04% vs 5-15%). Consequently, there will be higher energy consumption for CO_2 uptake in DAC compared to other techs.

For the thermodynamical analysis of DAC, it is enough to take into account the mixtures of ideal gases. At component partial pressures below 1 atm and ambient temperatures, ideal gases can be a helpful tool for describing the air and its components.

$$G_{\text{mix}}\left(P_0, P_{CO_2}\right) = RT \left(\frac{P_{CO_2}}{P_0} \ln\left(\frac{P_{CO_2}}{P_0}\right) + \frac{P_0 - P_{CO_2}}{P_0} \ln\left(\frac{P_0 - P_{CO_2}}{P_0}\right)\right) \qquad (2.9)$$

Formula 2.9 reflects the Gibbs free energy for mixing 1 mol of a two-component gas (CO_2 and CO_2 -free air), where P_0 is the ambient pressure; P_{CO2} is the partial pressure of CO_2; T is the ambient absolute temperature, and R is the universal gas constant.

For the complete separation of the input gas into pure CO_2 and CO_2-free air, the free energy of mixing should be learned. In this case, the free energy is known as the theoretical minimum for the separation process. Generally, work needed for the separation process is equal to -ΔG, and the most appropriate way for capturing CO_2 would be skimming the stream for the highest possible concentration of CO_2 rather than scrubbing the gas stream entirely.

After some simplifications carried out, Formula 2.10 can be achieved for calculating the minimum work needed for the extraction of 1 mol of CO_2 from the mixture [28]:

$$W = RT \left| \ln \frac{P_1}{P_0} \right| \tag{2.10}$$

2.4.5 Regeneration of adsorbents in DAC

Generally, the most common direct air capture with carbon storage utilizes solids that apply an adsorption process rather than absorption. The adsorption is done in 2 steps. At the first step, CO_2 is adsorbed, while at the second step desorption process is implemented. Through pressure swing adsorption (PSA), temperature swing adsorption (TSA), or vacuum swing adsorption (VSA), the separation process of CO_2 and thereby the regeneration of the sorbent can be attained.

On the contrary to the absorption process, in the adsorption process, less energy is demanded to separate CO_2 from the amine sorbent. The best explanation is that in the adsorption process, there is a feebler bond between CO_2 and sorbent [23].

2.5 Adsorbent materials

There are quite a few groups of adsorbents for carbon capture that have been profoundly surveyed. Porous solid adsorbent materials, zeolites, metal-organic framework (MOF), zeolitic imidazolate framework (ZIF), activated carbons, amine-containing mesoporous materials, metal oxide carbonates, perovskites, hydrotalcites, and clathrate hydrates are good samples for it [29] [30].

Based on the adsorption condition, numerous materials have been investigated and pondered to acquire the maximum feasible efficiency for the CO_2 uptake technologies from ambient air.

At low-pressure conditions, membrane separation techniques have been used for CO_2 uptake. However, these techniques usually suffer from high operating expenses, and they are not energy-efficient enough to compress the feed gas [31].

Solid and liquid sorbents are the methods that can contribute to a "negative carbon emission" environment [26]. Solid-state materials are more practical for CO_2 capture considering their cost-effectiveness, ease to design, functional surface, energy-friendly, hydrophobicity, readily operable, and most significantly, easy regeneration of adsorbents [32].

Among the above-mentioned adsorbent materials, activated carbons and zeolites are the most frequently applied solid adsorbents for CO_2 capture. However, as the world evolves and gets more contemporary, different materials such as MOFs, metal oxides, and polymers are being studied and designed to augment CO_2 adsorption effectivity [33]. Cutting-edge analyses have also shown the utilization of cut-price materials derived from industrial and agricultural wastes like biochar from bagasse, coal fly ash, and biomass-based materials [30]. Figure 2.15 below illustrates the escalating interest in CO_2 uptake on solid materials.
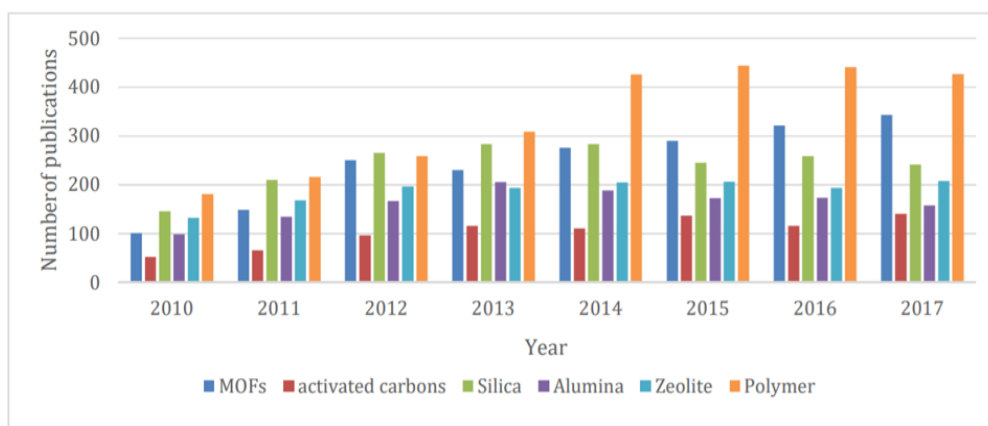
Figure 2.15: Increasing rate of publications on CO_2 capture with different solid sorbents [33].

2.5.1 Zeolites

Zeolites (also denoted molecular sieves) are a class of hydrated aluminosilicate minerals built from interconnected tetrahedra of alumina (AlO_4) and silica (SiO_4) through shared oxygen atoms. The Swedish mineralogist Axel Fredrik Cronstedt was the first who used the term

zeolite in 1756 [34]. Figures 2.16 and 2.17 below give a general overview of the chemical structure of the zeolite and its primary building unit. [35].
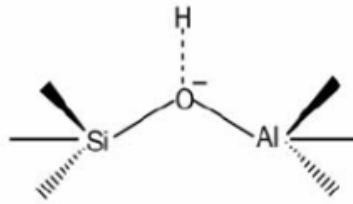
Figure 2.16: Chemical structure of the zeolite [35].
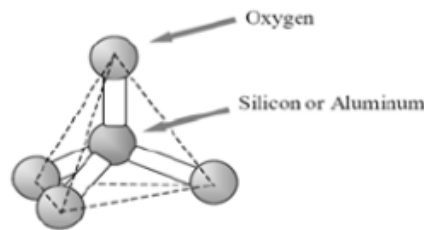
Figure 2.17: Primary building unit of zeolite structure [35].

Zeolites can be found in rocks of different ages, geologic settings, and lithology. Stilbite, mordenite, erionite, clinoptilolite, chabazite, heulandite, and phillipsite are among the most well-known types of zeolite [36].

Due to their unique porous structure and specific chemical composition, zeolites have been used in the different heaps of applications such as adsorption, separation, purification, catalysis. Moreover, zeolites own widely variable physicochemical properties, such as good thermal stability and ion exchange capability, and therefore are prevalently used for the CO_2 capture from the air [37].

The existence of aluminium atoms in silicate-based molecular sieve materials gives negative framework charges atoned with exchangeable cations in the pore space. These specific structural characteristics of zeolites make it feasible to adsorb a wide range of gas molecules and even acidic gas molecules such as CO_2 [34].

The main interest in zeolites for adsorption applications commenced in the 1960s. An infrared spectroscopy survey of CO_2 adsorption on the zeolites revealed that physisorption was the primary process in CO_2 adsorption on zeolites. Nonetheless, a negligibly small fraction of the adsorbed CO_2 (up to 0.15 mmol/g) was chemisorbed. Based on the assay carried out, it became

apparent that the physisorption was affected by the electric field due to the charge-balancing cations (in the pores) and by hydrogen bonding with surface silanol groups.

In other words, the CO_2 adsorption properties of zeolites were influenced by the aluminium content, which defines the number of charge-balancing cations in the structure.

It was also manifested that the base strength of zeolites expands with the aluminum content increment. The main reason for that is the lower electronegativity of aluminium relative to that of silicon. In a parallel effort to that, the increase in the basicity of the exchanged zeolites with the decrease in the electronegativity of the cations was also found out [34].

2.5.1.1 Zeolite classification

Zeolites can be both natural and synthetic originated. Natural zeolites are hydrothermal, and their origin is usually volcanic. Natural zeolites own perfect selectivity toward heavy metal ions and ammonium ions [38].

Up to now, more than 50 naturally occurring species of zeolites have been identified. Morphological characteristics, chemical composition, crystal structure, effective pore diameter, natural occurrence are the parameters that can create a classification for zeolites.

In 1997, nomenclature for zeolite minerals had been recommended by 'International Mineralogical Association Commission on New Minerals and Mineral Names.' According to the report, the ratio of Si to Al is not sufficient for distinguishing zeolite species except for heulandite (Si:Al<4.0) and clinoptilolite (Si:Al≥4.0). Dehydration, partial hydration, and over-hydration are not enough either for zeolite recognition [36].

Despite that, based on many types of research by different scientists, it became unanimously accepted that the Si to Al ratio is a notable characteristic of zeolites. The charge imbalance created owning to aluminium in the zeolite framework defines the ion-exchange characters of zeolites. The ratio of Si to Al is directly proportional to the thermal stability, whereas inversely proportional to the cation content. The surface selectivity varies from hydrophilic to hydrophobic if the ratio is getting more extensive [36].

The pore size and shape in a zeolite framework have an impact on the adsorption and catalytic properties and their capability for acting as a molecular sieve. Zeolite classification can be defined by the number of T atoms (T= silicon or aluminium ion) [39]. More generally, zeolites can be classified based on the silica/alumina ratio as below [36]:

•Zeolites with low Si/Al ratio (1.0 to 1.5)

•Zeolites with intermediate Si/Al ratio (2 to 5)

•Zeolites with a high Si/Al ratio (10 to several thousand).

Edith Marie Flanigen, an American chemist, has divided zeolites into different classifications based on pore diameter. Classification comprises of a small-pore zeolites, medium-pore zeolites, large-pore zeolites, and extra-large-pore zeolites [36]:

1) Small-pore zeolites (8-rings) with a free pore diameter of 0.3–0.45 nm

2) Medium-pore zeolites (10-rings) with a free pore diameter of 0.45–0.6 nm

3) Large-pore zeolites (12-rings) with a free pore diameter of 0.6–0.8 nm

4) Extra-large-pore zeolites (14-rings) with a free pore diameter of 0.8–1.0 nm.

ZSM-5 Zeolite is a good example of 10-ring zeolites. Zeolites X and Y belong to the large-pore zeolite groups because of the 12 rings present. Figure 2.18 below illuminates the structure of pores in some zeolites showing the 8-ring, 10-ring, and 12-ring shapes [39].
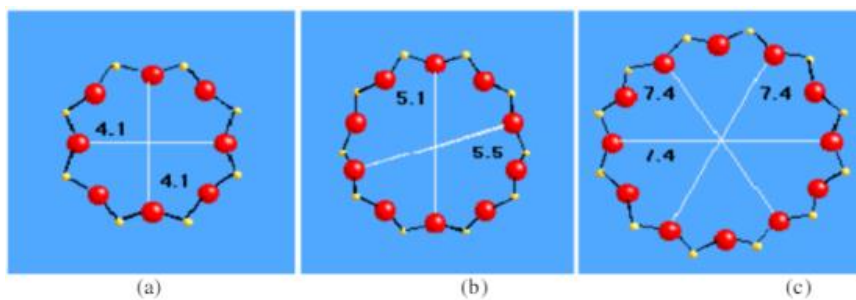
Figure 2.18: The structure of the pores in some zeolites showing (a) an 8-ring, zeolite A (b) a 10-ring, ZSM-5 (c) a 12-ring, zeolite Y [39].

Table 2.3 below illustrates the general classification of zeolite structures :

Number of linked tetrahedra	SBU created	Shorthand description
4	4oxygen ring	S4R
5	5oxygen ring	S5R
6	6oxygen ring	S6R
8	8oxygen ring	S8R
8	4-4oxygen rings	D4R
12	6-6oxygen rings	D6R
16	8-8oxygen rings	D8R

Table 2.3: Classification of zeolite structures (S=single, D=double, R=ring) [39].

2.5.1.2 Zeolite kinetics

Alongside the adsorption capacity, the kinetics of the CO_2 adsorption and desorption are overly crucial to the efficacy of the CO_2 capture platform. The CO_2 adsorption kinetics are more commonly pointed by the uptake curves. In the uptake curve, the change in the quantum of adsorbed CO_2 is shown as a function of time elapsing. In a preliminary work done by Barrer, the uptake curve of the microporous particles was outlined in terms of diffusion model, assuming the system was under isochoric and isothermal conditions [34].

For the CO_2 capture process by adsorption using zeolites, the adsorption process is incompatibly faster in the inception stage, entailing the material to fill almost the whole capacity just within tens of seconds. The adsorption kinetics can be influenced by operating states and highly dependent on temperature and pressure adjustments.

The isothermal capture model has been widely used by researchers to identify the CO_2 uptake curves of zeolites during the adsorption process. For instance, by dint of this approach, Rees succeeded in modeling carbon dioxide uptake rates of NaA (LTA) zeolite. It became clear that the adsorption rate was very swift at a temperature range between 273 and 388 K (Figure 2.19).
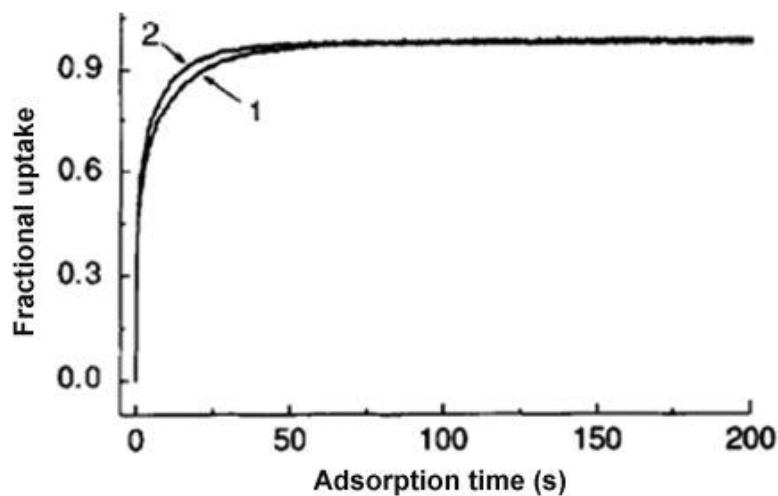
Figure 2.19: CO_2 adsorption rate of NaA zeolite at different temperatures (P=0.13 bar), 1: 323 K, 2: 388 K [34].

Furthermore, Aguilar-Armenta showed the uptake curves of CO_2 on erionite natural zeolite at two temperatures, 273 and 293 K (Figure 2.20).

Based on the achieved results, adsorption at both temperatures took place very impetuously, attaining more than seventy percent of the total capacity in the space of the first 20 seconds. [34] [40].

25
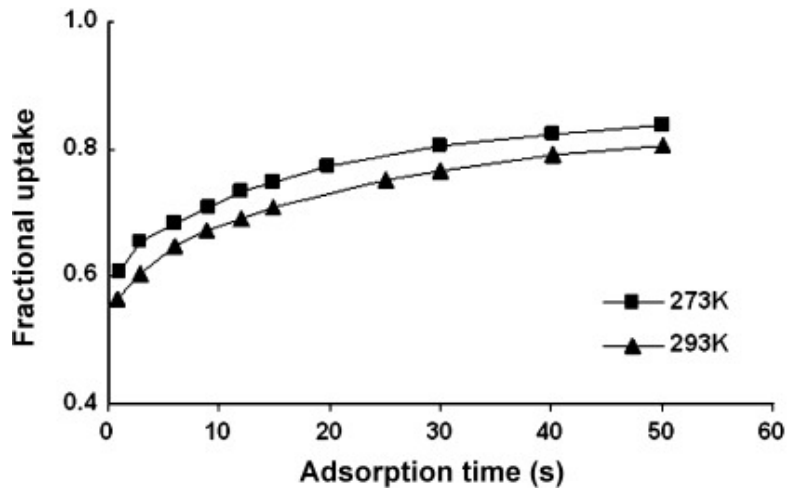
Figure 2.20: CO$_2$ uptake curves on erionite at 273 and 293 K [34].

Notwithstanding, this approach is not valid for some zeolites. For instance, based on Yucel's survey, CO$_2$ adsorption in zeolite 5A did not show an isothermal behaviour, and therefore, capture curves could not be examined by the model mentioned above. For clarifying the adsorption process in that case, the researchers suggested a non-isothermal model by taking the heat effects into account together with assuming that micropore diffusion through the crystals took domination in the overall mass transfer [34].

To put it all together, CO$_2$ adsorption kinetics on zeolites can be evaluated among the quickest known, getting their equilibrium capacity in less time than other materials [34].

2.5.1.3 Zeolite regeneration

In comparison to other inorganic adsorbents (hydrotalcites, metal oxides, etc.), zeolites are considered highly regenerable materials. Zeolites can renovate their adsorption capacities without necessary degradation even after abounding cycles of adsorption and desorption. PSA and TSA are the leading technologies that can be applied for the regeneration of zeolites [34].

According to the report by Aguilar-Armenta, a small amount of irreversibly adsorbed CO$_2$ on three natural zeolites, namely, ZAP, ZNT, and ZN-19, was seen.

For apprehending the regeneration of those zeolites, total and reversible isotherms were compared. The adsorbents were in a vacuum condition and without any temperature change. [34] [41].
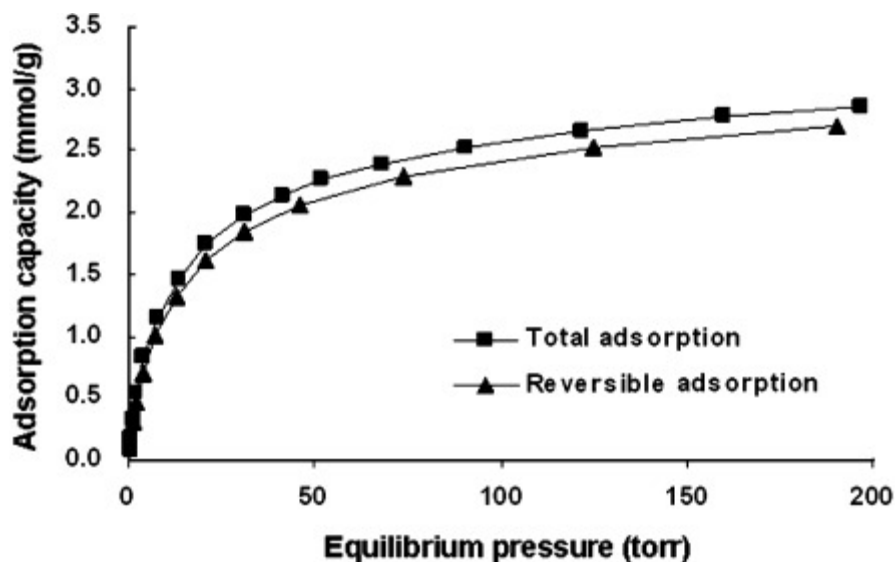
Figure 2.21: Adsorption of CO_2 for virgin and regenerated natural zeolite, ZAPS (ERI), measured at 298 K [34].

As can be seen from figure 2.21, a tiny amount (less than 0.5 mmol g^{-1}) was not regenerable (or irreversible) after the regeneration process applying PSA under constant temperature (298K) conditions.

Another test carried out by Siriwardane on the reversibility of adsorbed CO_2 was onto zeolites 13X. The test was run at 295 K and 17 bar pressure with 15% CO_2 under moist conditions.

It was revealed that its working capacity dwindled approximately from 6 to 4 mmol g^{-1} after two adsorption and desorption cycles. The small amount of chemisorption of CO_2 species was pointed out as a primary reason for such a scenario. Despite that, this amount of non-desorbed CO_2 was negligible, and that irreversibility could readily be eliminated by augmenting the temperature above 393 K.

Moreover, according to Tezel's report, the CO_2 adsorption capacity could be restored entirely with minor changes in isotherms by regenerating the adsorbents at 473K.

These surveys confirm that TSA would be a better solution than PSA for the recovery of a small amount of adsorbed CO_2 on zeolites [34].

2.5.2 Silica Gel

During the CO_2 capture process by adsorption, the removal of moisture is overly significant. In the experimental part of this thesis project, zeolites are used for CO_2 removal, while silica gel is used for water removal.

Silica gel owns an amorphous microporous structure, and its pore opening size varies between 3-60 angstroms. It is referred to as a colloidal form of silicon dioxide (SiO_2), and its interconnected pores with a high surface area are very attractive for adsorbing the water.

Zhang et al. tested ten different desiccant materials for air dehumidification processes and figured out that, in comparison to other materials, regular density silica gel (RD) and silica gel 3A showed tangibly better results [42].

Alahmer et al. investigated the characteristics of high-wound silica gel (WSG) and molecular sieve (LT3) desiccants. According to his report, when the relative humidity RH% of the air is above 60%, WSG is significantly better. In contrast, if the RH% of the inlet air is less than 50%, then LT3 desiccant is better. The adsorption isotherm in Figure 2.22 below illustrates the ability of these desiccants for moisture removal [43].
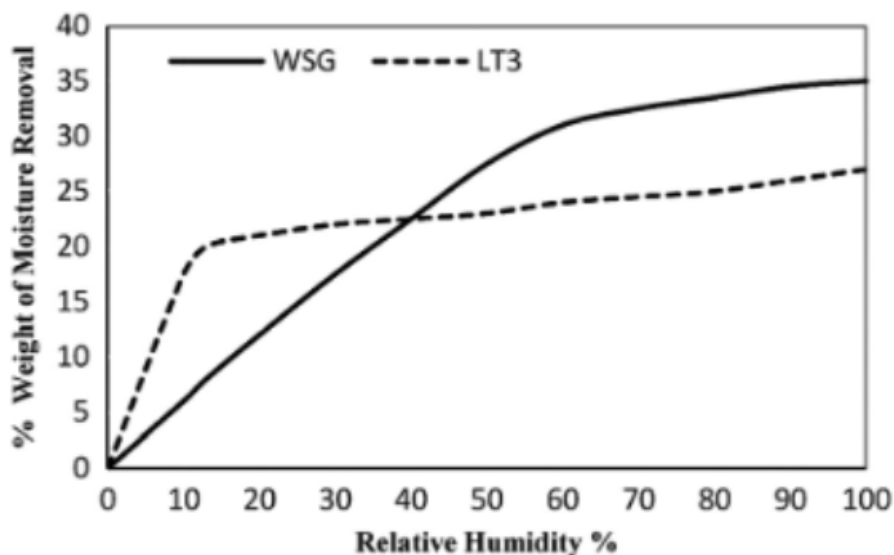
Figure 2.22: Isotherm curves for the WSG and LT3 desiccants at 25 °C [43].

3. Experimental Part

3.1 Experimental methodology

This experiment aims to delineate the CO_2 capture process on the Z8 test plant. The observation of the capture rates based on the shape of breakthrough curves, the determination of the amount of CO_2 captured both at breakthrough and the completion of the test, discussion of the pressure drop over the packed bed, and finding out the optimum working condition are the core of this experiment.

3.2 Adsorption materials

In this experiment, three different sizes of zeolite 13X and one specific size of silica gel W127 were used. Zeolites were used for the CO_2 capture process, while silica gel was deployed for moisture removal from the air before carbon removal.

For zeolite 13X, the pore openings in the crystals have a diameter of approximately 10 Å (angstroms). The bead sizes of zeolites were on average 2 mm for small size, 4 mm for medium size, and 6 mm for big size.

The datasheets concerning the properties of adsorbents have been taken from Greencap Solutions and can be found in Appendix C.

3.3 Plant set-up and major equipment

The experiments were carried out using the Greencap Solutions (GCS) Z8 plant. The general test facility view is represented in Figures 3.1 and 3.2 below.

Figure 3.1: The front-side view of the Z8 test plant

Figure 3.2: The back-side view of the Z8 test plant

Visibly, there are three adsorption columns, namely, 1st water adsorption column (C-101), the CO_2 adsorption column (C-102), and 2nd water adsorption column (C-103). The CO_2 capture process is implemented based on the TSA principle.

The setup is based on a back-and-forth process, meaning that if adsorption occurs in one direction, then the desorption will arise in the opposite direction. The Z8 plant is composed of abundant utensils for different purposes. They can be divided into air inlet system, adsorption/desorption columns, solenoid valves, heaters, and exhaust system containing various instrumentations and controls themselves.

3.3.1 Air inlet system

Air inlet system comprises of the several instrumentations and controls as below:

1) Temperature transmitter indicator to display inlet air temperature locally
2) Self-regulating pressure control valve to decrease inlet air pressure from 8 bar down to 2 bar
3) Venturi flow meter with indicator and transmitter to show inlet air flow rate
4) Inlet air water cooler
5) The inlet expansion enclosure containing:
   a) Temperature transmitter indicator to illustrate inlet air temperature
   b) CO_2 analysis transmitter indicator to illustrate CO_2 concentration
   c) Relative humidity analysis transmitter indicator to present relative humidity

3.3.2 Water and CO_2 adsorption columns

The test plant consists of two water adsorption columns and one CO_2 adsorption column. These adsorption columns themselves also contain several instruments for the process control system. These instruments are installed to the top, middle, and bottom of each adsorption column.

Instruments attached to the top of the column:

1) Relative humidity analysis indicator
2) Temperature indicator transmitter
3) Pressure indicator transmitter
4) Sampling valve to use for taking gas samples for manual analysis

An instrument attached to the middle of the column:

1) Temperature indicator transmitter

Instruments attached to the bottom of the column:

1) Relative humidity analysis indicator
2) Temperature indicator transmitter
3) Pressure indicator transmitter
4) Sampling valve to use for taking gas samples for manual analysis

3.3.3 Solenoid Valves

These valves are on/off two-way valves that can be set to divert inlet and outlet in the system by deploying logical interlocks. HS-101 to HS-104 and HS-106 to HS-108 solenoid valves to control airflow during adsorption and desorption cycles.

3.3.4 Heaters

In total, there are three heaters for desorption and regeneration purposes of the columns. First, the temperature element measures the temperature of heated air at the outlet of the heater and sends it to the local temperature indicator controller. The controller compares the measured temperature with the set-point temperature (200 °C) and dispatches the signal to the solid-state regulator to adjust the power input to the heater.

During an adsorption process, the heater in the C-103 column is turned on to regenerate the column packed with silica gel and prepare it for the desorption process. In the space of the desorption process, two heaters will be switched on, namely in the C-101 and C-102 columns, to desorb CO_2 and water and make it ready for the subsequent runs.

3.3.5 Exhaust system

The air outlet system contains the below-mentioned instrumentations and controls:

1) Sampling outlet air water cooler
2) Venturi flow meter to display outlet air flow rate
3) Expansion enclosure

3.4 Experimental procedures

The first step of starting the experimental procedures is about filling the columns with adsorbent materials. Adsorbent materials are kept in properly closed barrels to prevent air leakage and reduce their adsorption capacity. Having filled the columns with zeolite and silica gel, each part of the Z8 test plant was scrutinized visually for safety issues.

Subsequently, the flowrates were calculated for entering the values on the Programmable logic controller (PLC) display of the Z8 test plant. The formula used for the calculation of flowrates is as below:

$$Q = v \cdot A \tag{3.1}$$

Where:

v= superficial air velocity, A= cross-sectional area.

Regarding the column details, the column length is 1500 mm (OD=219.1 mm, thickness 3.76 mm, ID=211.58 mm), and the length of the packed bed is 350 mm.

The experimental procedure starts with the adsorption process and is followed by desorption for the regeneration of the adsorbents.

3.4.1 Adsorption process

For the startup of the adsorption process, the compressor was turned on, connected to the air inlet system via a hose, desired inlet temperature and flowrate were defined on the PLC display, the manual air inlet valve was opened, and eventually, the adsorption process was ready to run.

The figures below (3.3 and 3.4) illustrate the general view of the air compressor and the process flow sheet of the adsorption process.

Figure 3.3: Air compressor
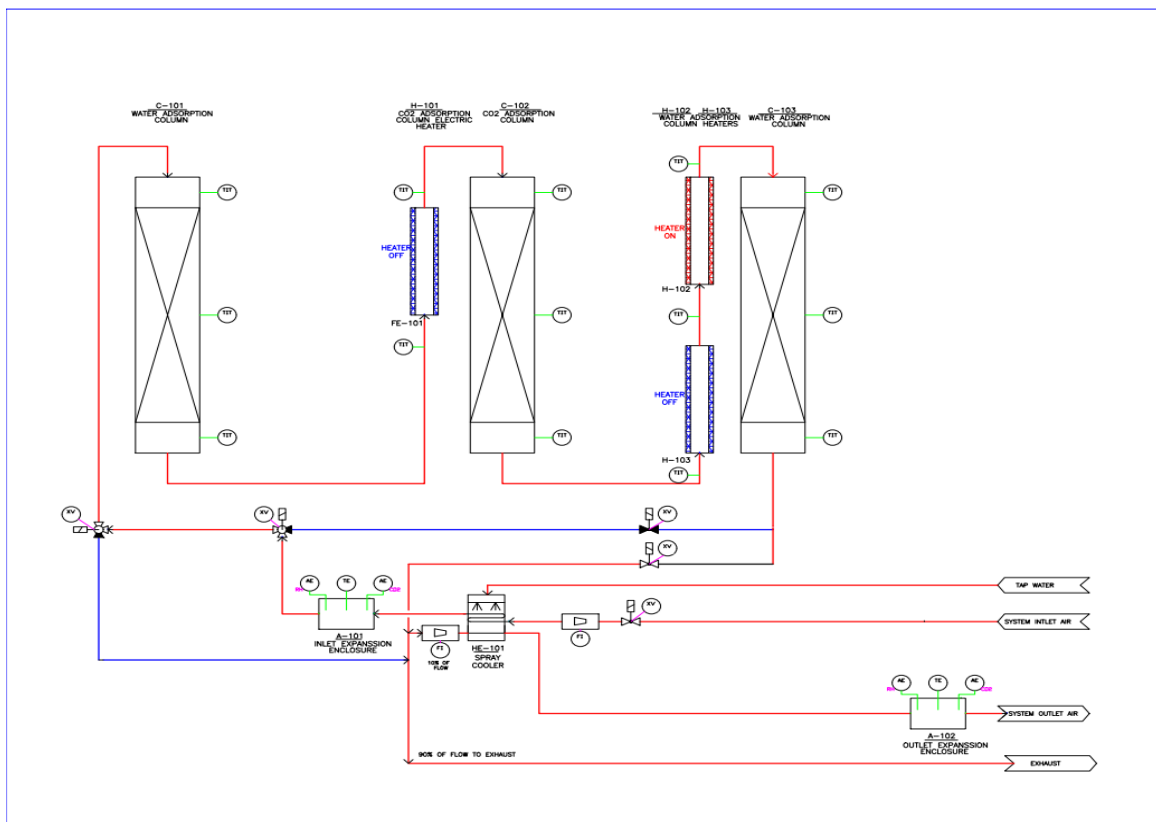
Figure 3.4: PFD of the adsorption process

The compressor grabs air from the ambiance and compresses it up to 8 bar, then fed to the air inlet system. Then, after passing through the specific instruments explained above, the grasped air is directed towards the 1st water adsorption column (C-101) before being introduced to the CO_2 adsorption column (C-102). In C-102, almost water-free air flows, and CO_2 is captured on the surfaces of the zeolites. Afterward, CO_2-free air flows to the C-103 column, which is then released into the atmosphere.

It is very significant to have water removal before the air is fed to the CO_2 adsorption column. The main reason is that zeolites are also very high selective towards H_2O, and even a trace amount of water vapor can drastically decrease the CO_2 adsorbing capacity.

As far as this is a back-and-forth process, there are two adsorption beds with a layer of silica gel followed by one zeolite bed. Thus, if in the adsorption process, the air flows in sequence from C101→ C102 → C103 columns, then in the desorption process, it should be in C103 → C102→ C101 sequence. At the expense of the silica gel, water can be mostly removed from the feed air and then dispatched to the next column (C-102), which concerns almost the water-free CO_2 adsorption process.

Simultaneously, during an adsorption process, 2nd water adsorption column (C-103) was heated by the heater H-102 to dehumidify the silica gel and make it ready for the desorption process. Each time, after reaching the equilibrium capacity (around 440-450 ppm at the outlet of the packed bed), the adsorption process was halted.

Moreover, the setup of solenoid valves (self-adjustable valves) was visually scrutinized to run a safe experiment. The sequence of solenoid valves should be according to Table 3.1:

Tag Number	Adsorption
XV-101	On
XV-102	Off
XV-103	On
XV-104	Off
XV-105	On
XV-106	Off
XV-107	Off
XV-108	On

Table 3.1: The sequence of solenoid valves in the adsorption process

3.4.2 Desorption process

Before starting the desorption process, it is necessary to turn the H-102 heater off and wait until the C-103 column cools down to 20 °C. When the desorption process commences, the loop will be in a reverse direction, and by applying the TSA principle, heating the CO_2 and 1st water adsorption columns (C-102 and C-101) by H-101 and H-103 heaters, the regeneration of zeolites becomes plausible. Eventually, separated CO_2 can be stored or released to the surrounding. The flow diagram of desorption is shown in Figure 3.5 below:
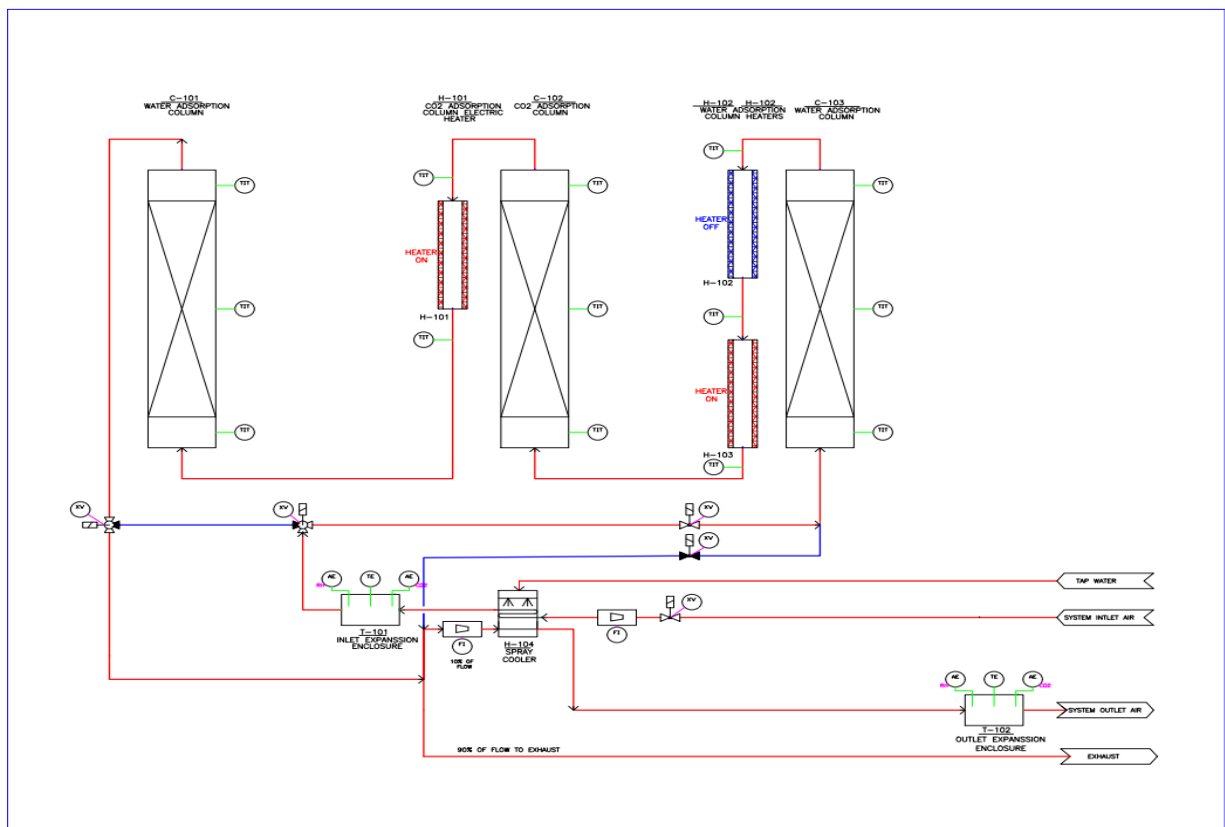
Figure 3.5: PFD of the desorption process

The sequence of solenoid valves during the desorption process should be according to Table 3.2:

Tag Number	Adsorption
XV-101	Off
XV-102	On
XV-103	Off
XV-104	On
XV-105	Off
XV-106	On
XV-107	On
XV-108	Off

Table 3.2: The sequence of solenoid valves in the desorption process

3.4.3 Desorption challenges

Ideally, full-cycle consists of adsorption, which is followed by desorption for the regeneration of adsorbents. Unfortunately, the desorption process did not go as planned because heaters could not heat the columns to the set-point temperature (200 °C). In Figure 3.6, it can be seen that during the adsorption process, though the set-point temperature at the inlet of the C-103 column was 200 °C, it never increased more than 94.5 °C (TIT 116). Thus, the regeneration of adsorbent materials was unsuccessful.

At first, the possible reasons were thought to be either the malfunction of temperature sensors or lack of power supply to the heaters. Both feasibilities were verified, where no problem was found.

For checking the temperature sensors, they were dismantled and put into the kettle with boiling water and a bucket full of ice. After verification, it became clear that the sensors operated properly. For the part of the power supply, it was verified by dint of amper-meter, where no problem was observed either.

Having faced such a challenge, it was decided to rerun the same experiment after the desorption to check the reliability of the desorption/regeneration process. Unfortunately, the breakthrough was observed in strikingly less time, which didn't coincide with the run carried out a day before.

Observing the breakthrough in a shorter time means that the adsorbent materials were not successfully regenerated. Such a problem took place repeatedly, which proved the failure of the desorption process and thus the regeneration of sorbents.

Finally, the core for such a problem was revealed to be isolation issues. Because of the inadequate insulation, heaters could not heat the columns to the set-point temperature, leading to the failure of the desorption process. Therefore, instead of doing the desorption and regeneration procedure, manual changing of sorbents was decided. In other words, after each run, the adsorbent materials inside the columns were substituted with fresh ones to run the experiments under the same working conditions.

During the manual change of materials, everything went successfully except relative humidity in the CO_2 adsorption column (AIT 109), which was not acceptable because it was even higher than the relative humidity at the inlet of the C-101 column (figure 3.6). Ideally, after passing through the C-101 column and removing moisture at the inlet of the C-102 column, relative humidity should be near zero.

Another problem was about the inlet temperature (TIT 110) of the C-101 column, where it should have been 10°C as the inlet air temperature was set to 10°C. However, because of the isolation issue, the temperature at the inlet of the C-101 column was equal to the ambient temperature (19.2°C) rather than 10°C (set-point).
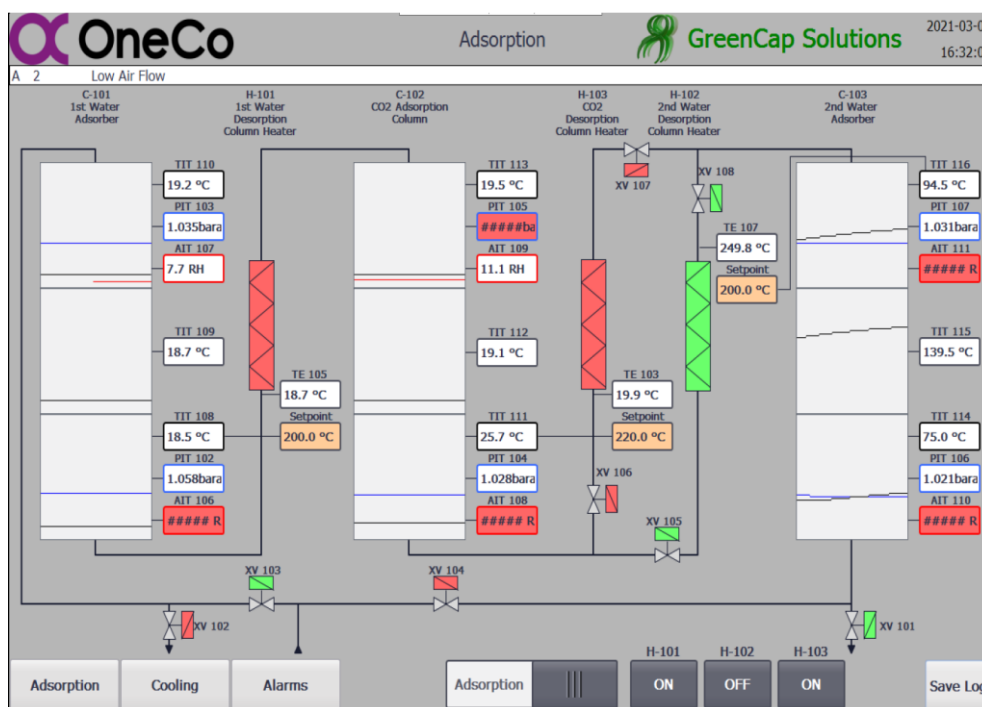
Figure 3.6: Screenshot from PLC display of Z8 plant

3.5 Data logging and measurement

The Z8 test plant has several sensors explained above, which constantly measure the temperature, pressure, and relative humidity of the columns.

In total, there are six sampling points at the bottom and top of each adsorption column. These bypass lines were used to measure CO_2 concentration and pressure drop over the packed bed. Figure 3.7 below gives a general look at the bypass lines.

The Kimo measurement device and differential pressure manometer were used additionally for data logging and measurement purposes.

Figure 3.7: Bypass lines from adsorption columns

3.5.1 Breakthrough detection

The Z8 plant itself contains a sensor that steadily measures the CO_2 concentration at the outlet of the packed bed in the CO_2 adsorption column. Despite that, to get more accurate data, the Kimo measurement device was also deployed.

A bypass line from the bottom of the CO_2 adsorption column was connected to the sampling bottle via a hose during an adsorption process. Then, the Kimo device was attached to the sampling bottle and continuously measured CO_2 concentration in the sampling bottle, which showed the CO_2 content at the outlet of the packed bed.

Kimo measurement device logs the data every 5 minutes, and until reaching the breakthrough, CO_2 concentration shows 0 ppm on the display of Kimo. However, after some time, the zeolite adsorption capacity decrements, and CO_2 is detected at the outlet of the packed bed; thus, a breakthrough observed. Initially, this concentration is low and increases over time until the CO_2 concentration in the feed air, and it trends a breakthrough curve. The breakthrough curve provides information about the adsorbent CO_2 storage capacity and the rate of CO_2 uptake.

Figure 3.8 below illuminates the Kimo device attached to the sampling bottle for a constant check of CO_2 concentration.
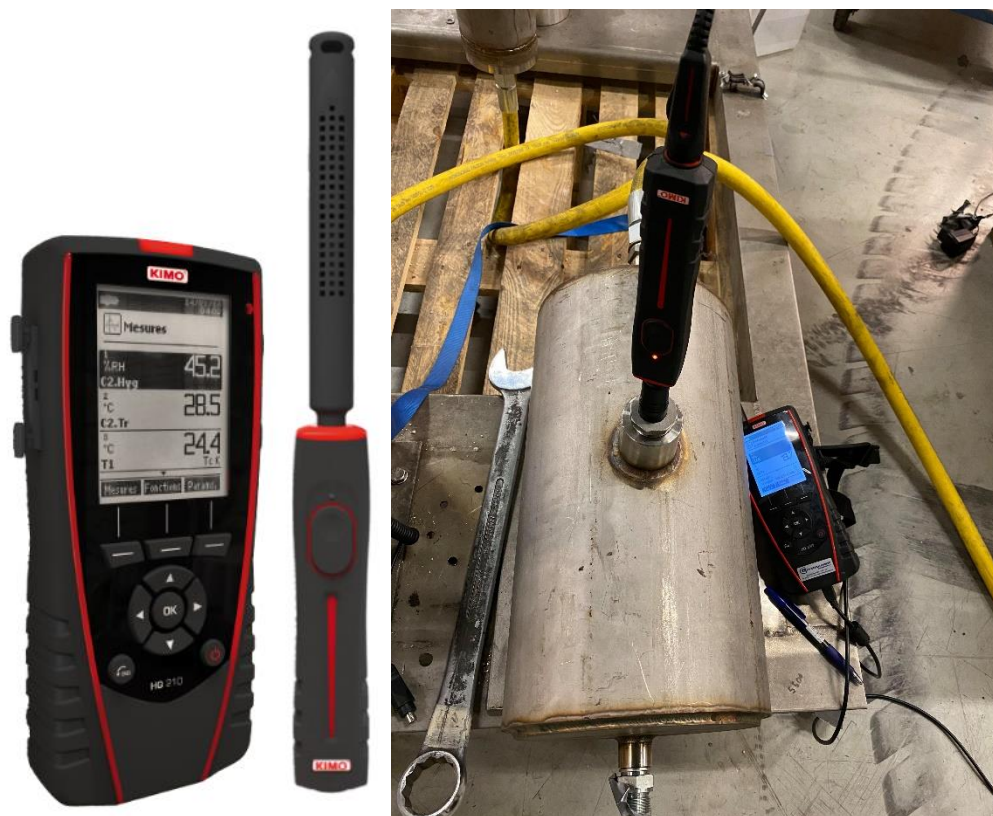
Figure 3.8: Kimo device connected to the sampling bottle

3.5.2 Pressure-drop measurement

The pressure drop measurement was also implemented using a bypass line, connecting two outlets from the CO_2 adsorption column (from the bottom and top of the packed bed) to a differential pressure manometer. The knowledge about pressure drop is utterly crucial as it influences the adsorption capacity.

Figure 3.9 shows the applied differential pressure manometer during experimental procedures.

Figure 3.9: Differential pressure manometer

4. Results and Discussion

4.1 Experimental investigation of CO_2 capture breakthrough curves

In total, 9 tests are presented to discuss the obtained results from the experiments. However, because of the arisen challenges during experimental procedures, 18 trials were carried out to acquire good results.

For each size of zeolite test (small ≈ 2 mm, medium ≈ 4 mm, and big ≈ 6 mm), the working conditions were the same, operating at ambient air temperature and applying three different superficial air velocities, namely, 0.2 m/s (low), 0.25 m/s (medium), and 0.3 m/s (high). The central motive is to figure out the significance of particle size and flowrate on the capture process.

The initial CO_2 concentrations in Figures 4.1-4.9 below are equivalent to that in the feed air. As soon as the adsorption process commences, a sharp decrease in CO_2 concentration inside the sampling bottle (the CO_2 concentration at the outlet of the packed bed) can be noticed, reflecting the success of the adsorption of CO_2 over the packed bed of zeolite beads. However, after some time, CO_2 will be detected at the outlet of the packed bed, initially at a very low concentration. The concentration is proportionally increasing with time, and the test proceeds until the CO_2 breakthrough curve is complete, or the concentration of CO_2 downstream the packed bed is the same as the concentration of CO_2 in the feed air.

4.1.1 Small size 13X zeolite

Low Air Flowrate Test 1.1

Figure 4.1 illustrates the breakthrough curve at 0.2 m/sec superficial air velocity (flowrate 25.3 m^3/h).
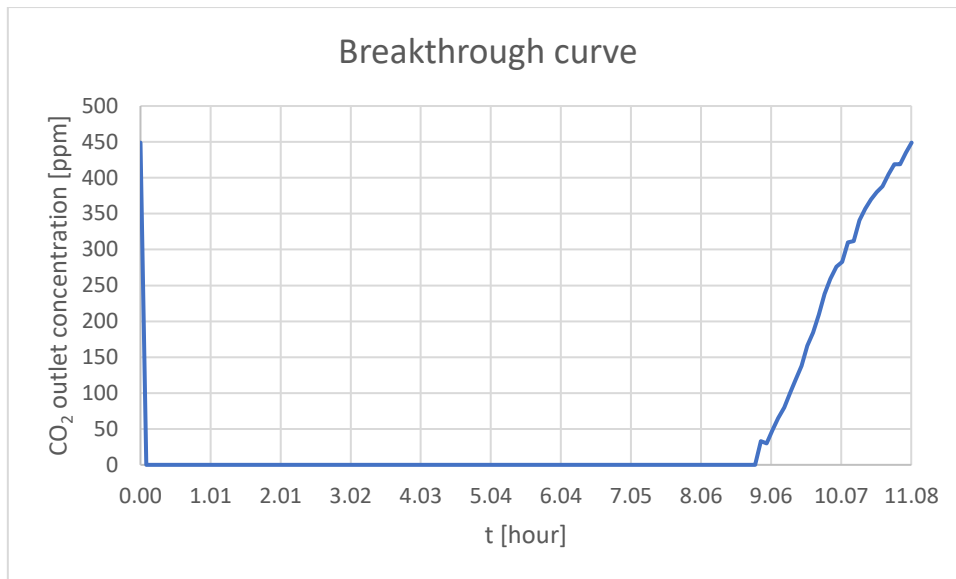
Figure 4.1: Breakthrough curve at 0.2 m/sec over small size zeolite

The breakthrough was observed in 8.92 hours, inferring that the adsorption efficiency was 100% during this period. After the time breakthrough was noticed, the efficiency starts to fall further until the end of the test. Ultimately, in 11.08 hours, the CO_2 concentration at the outlet of the packed bed was equal to that initially in the air (449ppm), meaning that the adsorbent media was not anymore capable of adsorbing CO_2 from the feed air.

Medium Air Flowrate Test 1.2

Figure 4.2 shows the breakthrough curve at 0.25 m/s superficial air velocity (flowrate 31.6 m^3/h).
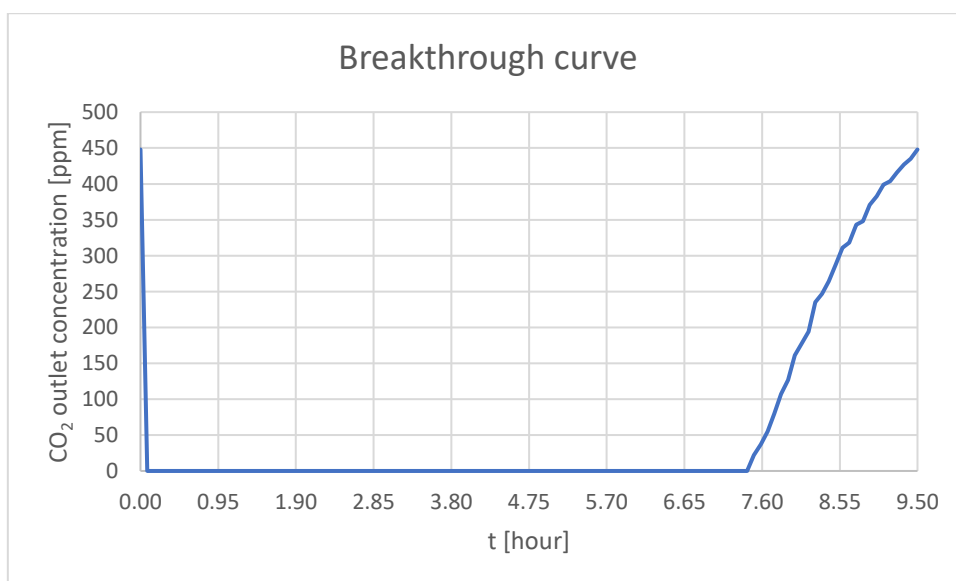
Figure 4.2: Breakthrough curve at 0.25 m/sec over small size zeolite

The breakthrough was noticed in 7.50 hours with this air flowrate, and it took 9.50 hours for a complete test. In this case, the CO_2 concentration in the feed air was negligibly less than in the first case, namely, 448 ppm vs. 449 ppm, and as the flowrate was comparatively higher, it took a shorter time to reach a breakthrough.

The higher flowrate increments the probability of the diffusion process on the surface of the particles. Till the breakthrough, the external diffusion is dominating, and consequently, the higher flowrate, the faster the adsorption rate is noticed.

High Air Flowrate Test 1.3

Figure 4.3 renders the breakthrough curve at 0.3 m/s (flowrate 38.0 m³/h) superficial air velocity.
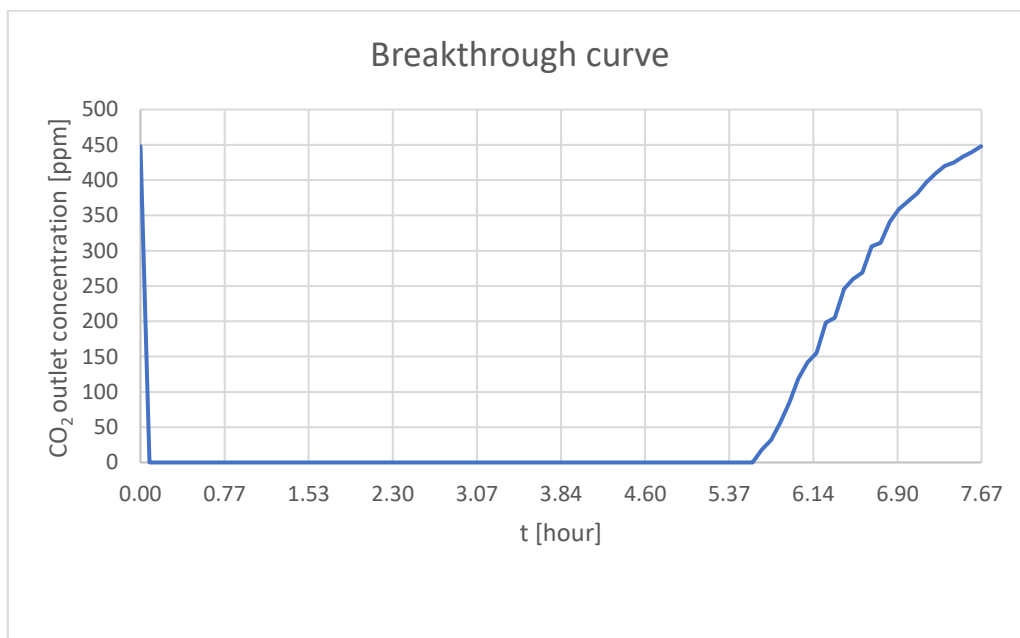
Figure 4.3: Breakthrough curve at 0.3 m/sec over small size zeolite

With this flowrate, the breakthrough was seen in 5.58 hours, while the duration of reaching the equilibrium adsorption was 7.67 hours (444ppm). This is the fastest capture rate obtained compared to that at lower flowrates. Here, the effect of flowrate can be easily discerned once more. So, the higher the flowrate, the higher the capture rate.

Last but not least, the time from breakthrough till the end of the test is almost the same for three different applied flowrates. This proves that the flowrate has a more significant impact on the capture rate until the breakthrough because most of the captured CO_2 is encountered during that period.

4.1.2 Medium size 13X zeolite test

Low Air Flowrate Test 1.4

The working conditions were kept the same as in the small-size zeolite tests. The only difference was about the size of zeolite for comprehending the size impact on CO_2 capture rate.

Figure 4.4 represents the breakthrough curve obtained at 0.2 m/sec over medium size zeolite.
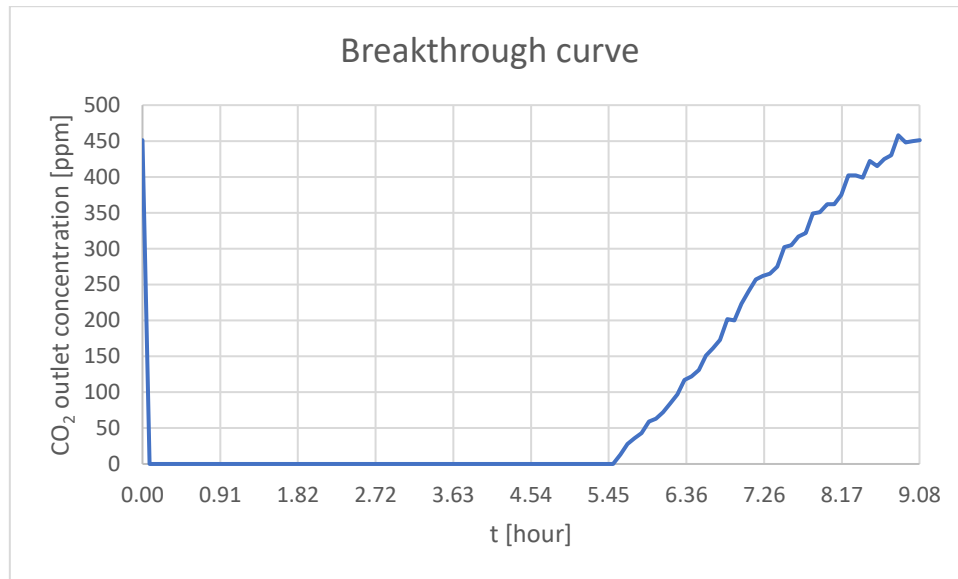
Figure 4.4: Breakthrough curve at 0.2 m/sec over medium size zeolite

The breakthrough was witnessed in 5.58 hours, and in 9.08 hours, the adsorption equilibrium reached (451 ppm). Relative to the small-size test (test 1.1), the capture rate until a breakthrough is 3.34 hours quicker. Regarding the complete test, it is 2 hours faster than the small-size zeolite. The principal reason for such a scenario is that as the particle size grows, the number of active sites on the surface area shrinks and causes a faster adsorption rate.

However, if we compare the time from breakthrough till equilibrium, we can observe that it took more time than test 1.1. The reason is that until the breakthrough, the external diffusion is dominant, while from the time breakthrough occurred till the equilibrium adsorption, the intraparticle diffusion becomes more prevalent. So, as the particle size gets bigger, it takes more time for internal diffusion and zeolites to be fully saturated with CO_2.

So, medium-size adsorbent at 0.2 m/sec showed a faster trend in capture rate than small-size, but less adsorption capacity.

Medium Air Flowrate Test 1.5

Figure 4.5 illustrates the breakthrough curve at 0.25 m/sec superficial air velocity over medium size zeolite.
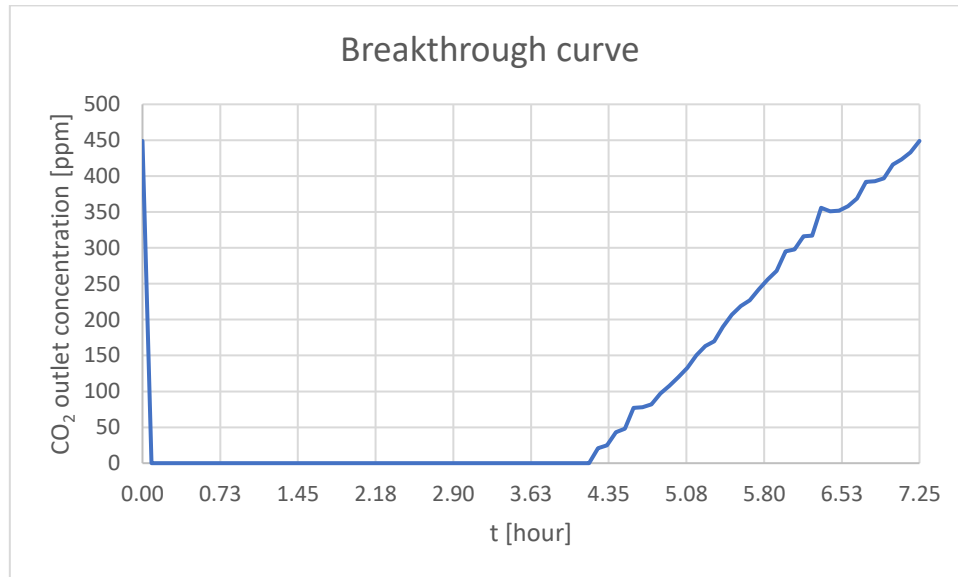
Figure 4.5: Breakthrough curve at 0.25 m/sec over medium size zeolite

In this case, the breakthrough was noticeable after 4.25 hours. Compared to the small-size zeolite (test 1.2), this is 2.25 hours faster in reaching the full adsorption capacity (or equilibrium), namely, in 7.25 hours. This scenario once more proves that the bigger size of zeolite saturated faster because of less contact surface area.

In contrast to the low flowrate medium-size zeolite (test 1.4), a faster scenario was observed both in respect of breakthrough and complete test duration. Higher flowrate and bigger particle sizes are the main reasons for it.

Nevertheless, in this test, the time from breakthrough until equilibrium is again strikingly more than in test 1.2 (3.00 hours vs. 2.00 hours).

High Air Flowrate Test 1.6

Figure 4.6 reflects the breakthrough curve at 0.3 m/sec superficial air velocity.
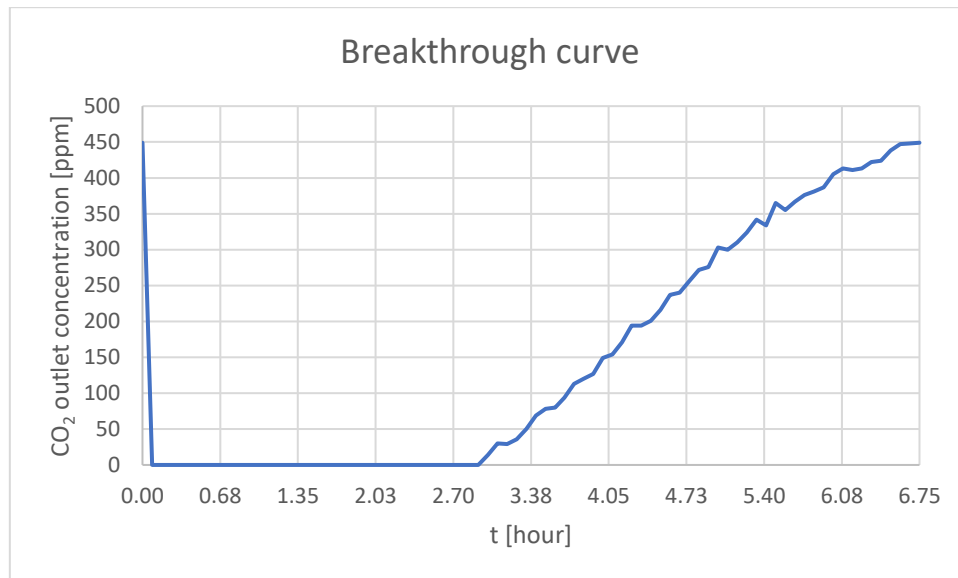
Figure 4.6: Breakthrough curve at 0.3 m/sec over medium size zeolite

In this case, the breakthrough observed in 3.00 hours which is 2.58 hours faster than that in the small-size (test 1.3), and in 6.75 hours, the adsorbent media became full of CO_2 and was no longer capable of adsorbing.

Relative to the small size zeolite (test 1.3), it took 0.92 hours less to reach equilibrium capacity. So, aside from the effect of sorbent particle size, as the flowrate increases, the difference in capture rates till breakthrough expands between small and medium-size adsorbents.

4.1.3 Big size 13X zeolite test

Low Air Flowrate Test 1.7

As in the previous (small and medium-size zeolite) cases, working conditions were kept the same with only the adsorbent size difference.

In Figure 4.7, the breakthrough curve for 0.2 m/sec superficial air velocity can be studied.
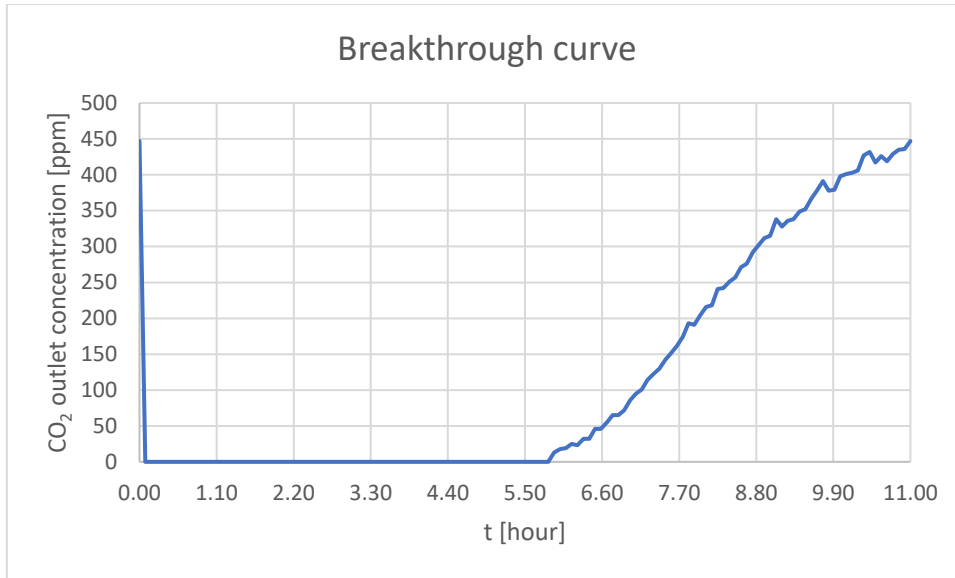
Figure 4.7: Breakthrough curve at 0.2 m/sec over big size zeolite

In this case, after 5.92 hours, the breakthrough was noted, and it took sharp 11.00 hours to reach the initial 447 ppm of CO_2, equilibrium adsorption. In comparison to small and medium-size zeolite, it trended almost the same scenario with small-size (test 1.1) in respect of complete test time, whereas in a medium-size zeolite (test 1.4), the full breakthrough curve was obtained strikingly faster.

Medium Air Flowrate Test 1.8

Figure 4.8 below shows the breakthrough curve at 0.25 m/sec.
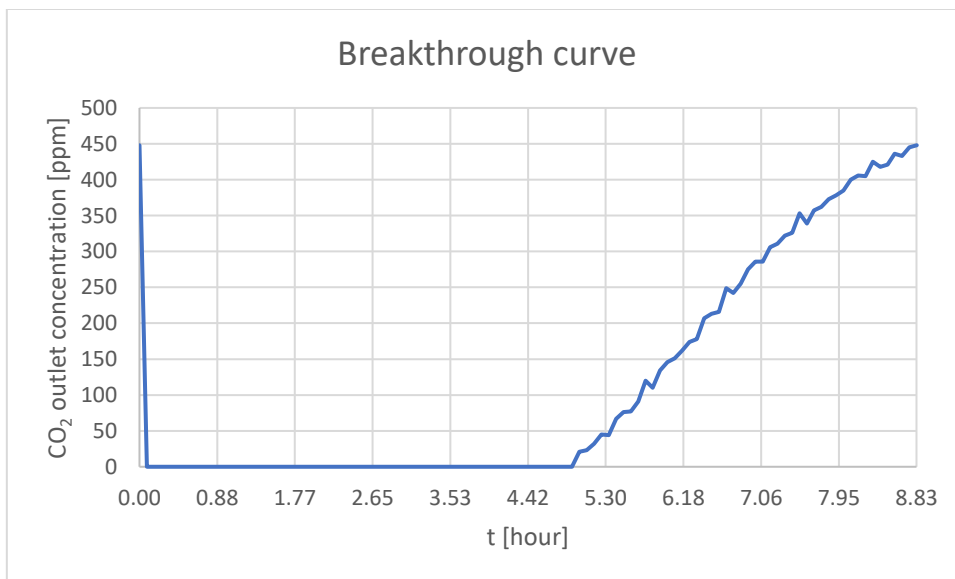
Figure 4.8: Breakthrough curve at 0.25 m/sec over big size zeolite

As the air flowrate is higher, the breakthrough is observed faster than in the 0.2 m/sec (test 1.7), namely 5.00 hours vs. 5.92 hours. Regarding the complete test, it took 8.83 hours vs. 11 hours. Compared to medium and small sizes, it reflected a faster capture rate than small size test 1.2, however slower than medium size adsorbent test 1.5.

High Air Flowrate Test 1.9

Finally, Figure 4.9 delineates the breakthrough curve at 0.3 m/sec.
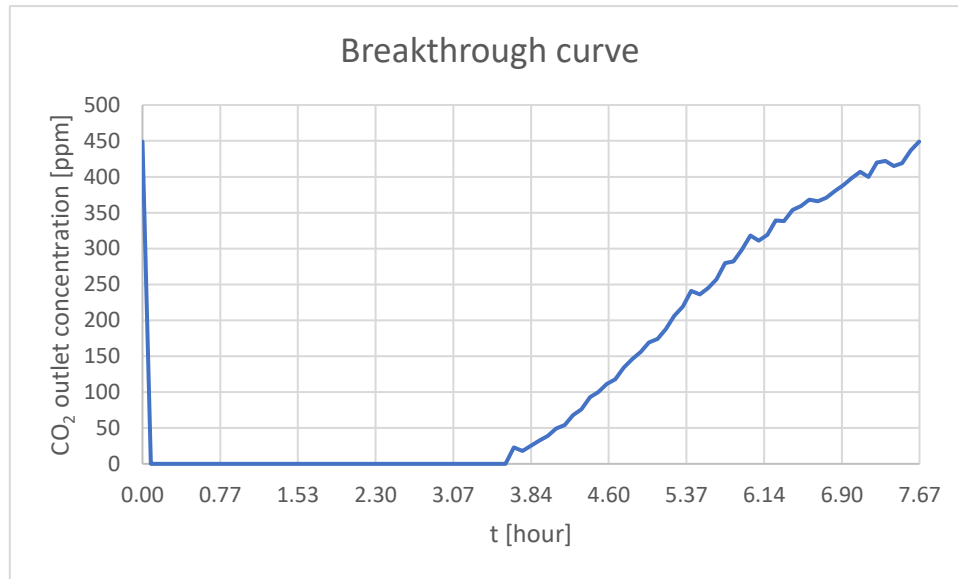
Figure 4.9: Breakthrough curve at 0.3 m/sec over big size zeolite

As it is predictable, at 0.3 m/sec superficial air velocity, the breakthrough observed quicker relatively to lower air flowrate cases. The breakthrough was observed in 3.67 hours, and in 7.67 hours, the initial (449 ppm) CO_2 concentration in air was acquired inside the sample bottle. To simplify the time respect, until breakthrough, it mirrored the faster capture rate than small size adsorbent (test 1.3) and slower than the medium size (test 1.6). Nonetheless, considering the complete test duration, it took the same time with the small size zeolite (test 1.3) but more time than medium-size.

In this test as well, the higher flowrate mainly has an impact on the rate till breakthrough rather than complete test duration. For a better comparison, Table 4.1 below has been attached. As can be seen, the longest time till breakthrough was seen in small-size tests because of owing more active surface area. More actives sides mean a longer time for external diffusion. However, the time-space from breakthrough till the end of the test shows a contrary trend. So, on average, for small size adsorbents, it took 2.08 hours, while for medium and big sizes, it

took 3.4 and 4.3 hours respectively from breakthrough till the equilibrium condition. The time for bigger particles to reach equilibrium adsorption (after breakthrough) is longer than the smaller size. Because, as the particle size increases, the path length expands as well, which causes a delay in the internal diffusion.

Particle Size	Test	Flowrate (m^3/h)	Breakthrough noticed (hour)	Complete test duration (hour)	Duration from breakthrough till equilibrium (hour)
Small	1.1	25.3	8.92	11.08	2.16
Medium	1.4	25.3	5.58	9.08	3.50
Big	1.7	25.3	5.92	11	5.08
Small	1.2	31.6	7.50	9.50	2.00
Medium	1.5	31.6	4.25	7.25	3.00
Big	1.8	31.6	5.00	8.83	3.83
Small	1.3	38.0	5.58	7.67	2.09
Medium	1.6	38.0	3.00	6.75	3.75
Big	1.9	38.0	3.67	7.67	4.00

Table 4.1: Summary of the CO_2 capture rate under different flowrates and sizes of zeolites

4.2 The captured CO_2 amount till breakthrough

The knowledge about the amount of captured CO_2 until the breakthrough time is utterly indispensable as it infers 100% efficiency. After the breakthrough, the efficiency decreases, and at equilibrium, it equals zero.

For calculating the adsorbed adsorbate amount until breakthrough, simple calculations were implemented as below:

1) Conversion of CO_2 concentration from ppm to mg/m^3
2) Multiplication of the CO_2 concentration (in mg/m^3) to the air flowrate to get the flowing (adsorbed) CO_2 amount over the packed bed in mg/h over the packed bed.
3) According to the breakthrough curve, the adsorption efficiency is 100 % till breakthrough. It allows calculating the captured amount of CO_2 by multiplying the time (till breakthrough) to the amount of CO_2 passing over the packed bed in an hour.

Table 4.2 summarizes all calculation steps and the amount of adsorbed CO_2 on the zeolite surfaces until breakthrough.

Particle size	Test	Flowrate (m³/h)	CO_2 concentration (ppm)	CO_2 concentration (mg/m³)	Time till Breakthrough (hour)	CO_2 flowing (mg/h)	Adsorbed CO_2 amount (mg)
small	1.1	25.3	449	808.2	8.92	20447	182387
small	1.2	31.6	448	806.4	7.50	25482	191115
small	1.3	38.0	448	806.4	5.58	30643	170987
medium	1.4	25.3	451	811.8	5.58	20538	114602
medium	1.5	31.6	449	808.2	4.25	25539	108540
medium	1.6	38.0	449	808.2	3.00	30711	92133
big	1.7	25.3	447	804.6	5.92	20356	120507
big	1.8	31.6	448	806.4	5.00	25482	127410
big	1.9	38.0	449	808.2	3.67	30711	112709

Table 4.2: Calculation of adsorbed CO_2 amount till breakthrough

Here, the effect of flowrate on the adsorption capacity can be easily discerned. The most captured CO_2 is encountered for small and big-size tests during medium flowrate tests (31.6m³/h).

However, as the flowrate increases further, the capture rate increases proportionally, and it entails less adsorption over the zeolites. It can be explained as the flowrate is higher, there is less residence time over the packed bed, and thus adsorbents have less possibility for capturing. In all cases, the least captured amount is seen during the highest flowrate tests.

Even though the small-size adsorbent was the slowest in respect of time, it has more adsorption capacity due to the larger specific surface area (or more active sides). As the particle size increases, the number of adsorbing sites decreases because of less surface area and leads to less adsorption capacity.

The strange scenario is that, compared to big-size zeolite, less adsorption capacity was observed in the medium-size zeolite. The possible reason is an improper distribution of particles in the packed bed and therefore being disturbed by the flow. Furthermore, differently from small and big-size zeolite tests, for medium-size zeolite, the most adsorbed CO_2 amount till breakthrough was observed in the lowest flowrate test 1.4.

4.3 The calculation of the captured CO_2 amount after the completion of the test

The calculation of the captured CO_2 amount until the complete test is more complicated, as it is hard to predict the efficiency after a breakthrough emerges. For determining the captured amount of CO_2 after breakthrough till equilibrium, regression analysis has been implemented to find the suitable mathematical model of the breakthrough curve. The following function 4.1 has been selected for the study:

$$f(t) = a \left(1 - e^{-t/b} \left(1 + \frac{t}{b}\right)\right) \tag{4.1}$$

This function is characterized by two constants, namely, a and b.

After obtaining the appropriate math model, the area below the curve has been calculated by finding the integral of the function. The integral of the function is as 4.2 below :

$$\int f(t)dt = a \left[t + b \cdot e^{-t/b} \left(1 + \frac{t}{b}\right) + b \cdot e^{-t/b}\right] - a(2b) \tag{4.2}$$

Proper values for a and b constants have been found by minimizing the root mean square error (RMC) in Excel using the solver feature.

The calculated area gives the feed-out or non-adsorbed (escaped) amount of CO_2. To find the total captured amount of CO_2, the difference of the feed-in and feed-out CO_2 amount should be found and added with the captured amount until a breakthrough (Table 4.2). It is evident that, at the termination of the test, namely in equilibrium adsorption, the concentration of CO_2 is equal to that in the feed air.

Figure 4.10 below shows the regression analysis for the small size zeolite test 1.3 (at 0.3 m/sec).
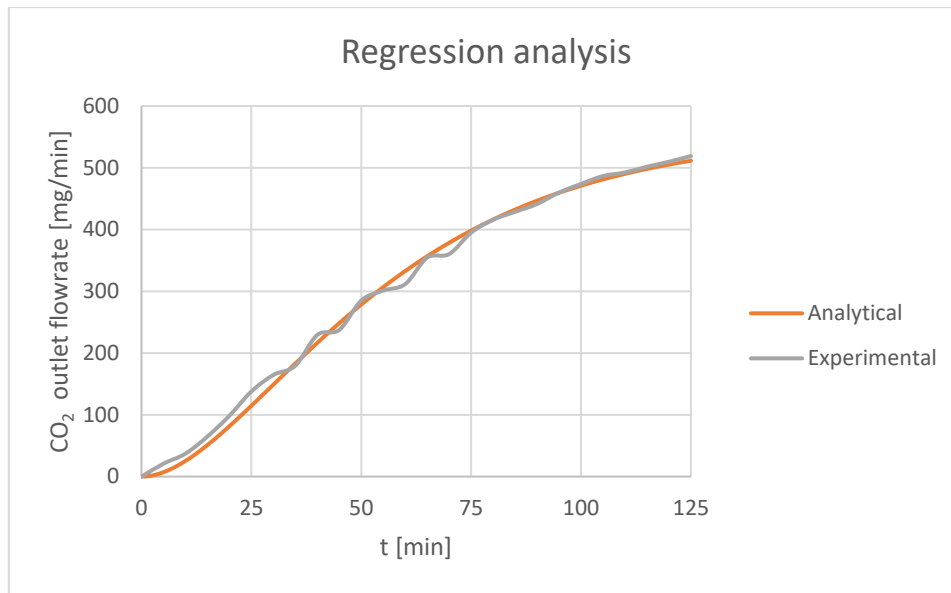
Figure 4.10: Regression analysis for test 1.3

The same type of analysis as in figure 4.10 has been fulfilled for each test (Appendix D), and the total amount of captured CO_2 for each test is as in table 4.3 below:

Particle size	Test	Flowrate (m³/h)	Adsorbed amount till breakthrough (mg)	Adsorbed amount from breakthrough till equilibrium (mg)	The total adsorbed amount (mg)
small	1.1	25.3	182387	20458	202845
small	1.2	31.6	191115	24501	215616
small	1.3	38.0	170987	27715	198702
medium	1.4	25.3	114602	38054	152656
medium	1.5	31.6	108540	41282	149822
medium	1.6	28.0	92133	56281	148414
big	1.7	25.3	120507	44149	164656
big	1.8	31.6	127410	52047	179457
big	1.9	38.0	112709	65635	178344

Table 4.3: Detailed overview of adsorbed CO_2 amount

Here, the interesting and quite different scenario is that, after the breakthrough, the effect of flowrate on the adsorption efficiency shifts. So that in all tests, from breakthrough to adsorption equilibrium, the captured amount of CO_2 increments with the increase of flowrate (calculated area). It can be deduced that as the internal diffusion is more dominant after breakthrough, a higher flowrate is more desirable for the efficiency of an internal diffusion process.

4.4 Pressure drops over the packed bed

Table 4.4 below summarizes the measured pressure drops (utilizing manometer) over the packed bed of zeolite 13X during the experiments at Greencap Solutions.

Particle size	Test	Flowrate (m³/h)	Pressure drop (kPa)
Small	1.1	25.3	0.254
Small	1.2	31.6	0.338
Small	1.3	38.0	0.445
Medium	1.4	25.3	0.213
Medium	1.5	31.6	0.237
Medium	1.6	38.0	0.397
Big	1.7	25.3	0.054
Big	1.8	31.6	0.076
Big	1.9	38.0	0.103

Table 4.4: Experimentally measured pressure drops over the zeolite 13X packed bed

Pressure drop is an inevitable case due to certain reasons, such as friction and wall roughness. Based on the table above and theory, as the bead size (particle diameter) increases, the pressure drop decreases. This can be explained as the void fraction is larger in bigger particles, it shows less resistance to the flow.

Furthermore, the higher the superficial air velocity, the bigger the pressure drop is observed. These impacts of the particle size and flowrate can be readily comprehended by the Ergun equation as well.

Ergun equation has been applied for the theoretical comparison of the obtained test results [44].

$$-\frac{\Delta P}{L} = 150 \frac{(1-\varepsilon)^2}{\varepsilon^3} \frac{\mu v_0}{D_p^2} + \frac{7}{4} \frac{\rho v_0^2}{D_p} \frac{(1-\varepsilon)}{\varepsilon^3} \tag{4.3}$$

Here, ΔP is the pressure drop, L - the length of the packed bed, ε - void fraction, μ-viscosity of air, D_p- particle diameter, and v_0- superficial air velocity, respectively.

Furthermore, ε (void fraction) was unknown, and the Dixon correlation has been proposed for predicting ε [45]. The correlation is as below:

$$\varepsilon = 0.4 + 0.05 \times \left(\frac{D}{d}\right)^{-1} + 0.412 \times \left(\frac{D}{d}\right)^{-2} \tag{4.4}$$

Here D is the internal diameter of the column, and d is the diameter of the adsorbent. Moreover, after predicting the void fraction of the packed bed, certain assumptions made as below for the application of the Ergun equation:

1) Viscosity through the packed bed is constant
2) The physical properties of the gas stream do not change after the removal of CO_2
3) As far as the temperature at the inlet and outlet of the C-102 column is different, the average viscosity selected
4) For each size of the zeolite, the average value for particle diameter calculated

4.4.1 Small size zeolite

Table 4.5 below illustrates the deviation of pressure drops between the experimentally measured and theoretical (based on the Ergun equation) values.

Superficial air velocity (m/sec)	Test	Experimentally measured ΔP (kPa)	ΔP calculated by Ergun equation (kPa)
0.2m/sec	1.1	0.254	0.281
0.25m/sec	1.2	0.338	0.385
0.3m/sec	1.3	0.445	0.503

Table 4.5: Pressure-drops in small-size zeolite

The deviation is an expected case, but the obtained results are very reasonable, which ratifies the proper distribution of particles in the packed bed.

Moreover, the table reflects the impact of flowrate on the pressure drop. So that, based on both experimental and theoretical data, as the flowrate increments, the increase in the pressure drop becomes evident.

Figure 4.11 designates the graphical relation between experimental and theoretical pressure drops. As it can visually be seen, the gradient of the pressure drop trends a linear shape.
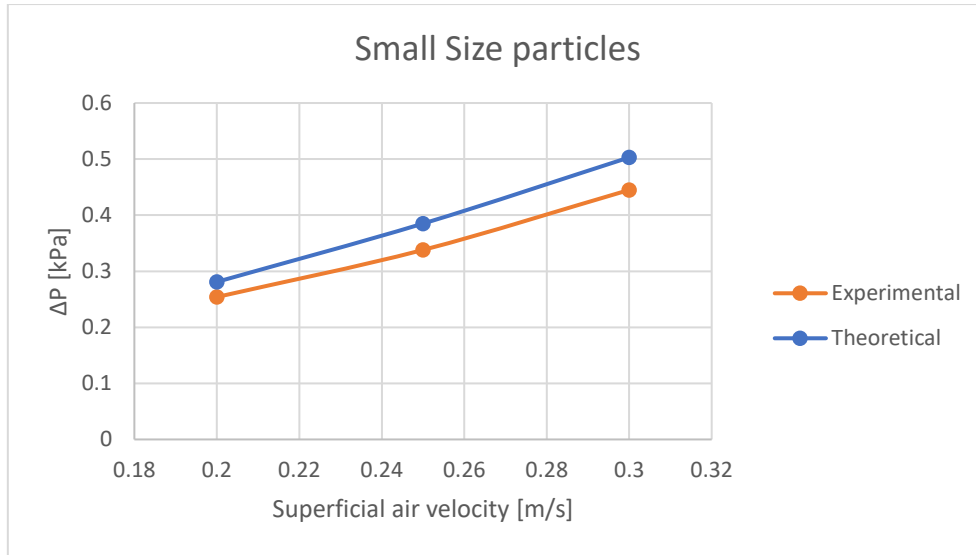
Figure 4.11: Pressure-drop evaluation over small-size zeolite

4.4.2 Medium size zeolite test

Superficial air velocity (m/sec)	Test	Experimentally measured ΔP (kPa)	ΔP calculated by Ergun equation (kPa)
0.2	1.4	0.213	0.134
0.25	1.5	0.237	0.189
0.3	1.6	0.397	0.253

Table 4.6: Pressure-drops in medium-size zeolite

As shown in Table 4.6, the pressure drops over the packed are less than in the first case (4.4.1), mainly because of the bigger particle size (4 mm against 2 mm), meaning a greater void fraction. However, for 0.3 m/sec (test 1.6), the experimentally obtained results don't trend a linear increase. The possible reason can be that there is maldistribution of the particles inside the column, which is detrimental to the packing efficiency, and thus, the packed bed is disturbed by the flow. In other words, blocking is a possible scenario at a high flowrate test because experimentally measured pressure drop is bigger than the theoretical.

Nevertheless, the tendency for the effect of flowrate is the same, meaning that higher pressure drops are imminent at higher flow rates. The only difference from small-size tests is that the increase in the pressure drop is not linear, which can be seen in Figure 4.12.
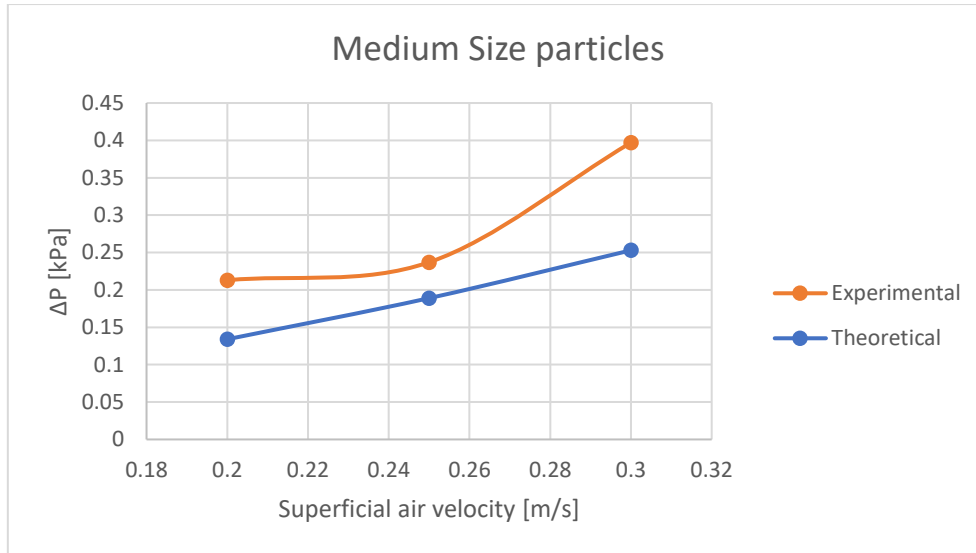
Figure 4.12: Pressure drop evaluation over medium-size zeolite

4.4.3 Big size zeolite test

In this case, the deviation between theoretically and experimentally measured pressure drops is the least, and the achieved results are very similar to each other (Table 4.7). This can be explained as the pressure drops are tiny compared to the cases mentioned above, and palpably, the deviation should be less.

Superficial air velocity (m/sec)	Test	Experimentally measured ΔP (kPa)	ΔP calculated by Ergun equation (kPa)
0.2	1.7	0.054	0.045
0.25	1.8	0.076	0.075
0.3m	1.9	0.103	0.101

Table 4.7: Pressure-drops in big-size zeolite

Furthermore, because of the biggest particle size compared to the two previous cases (4.4.1 and 4.4.2), and due to bigger void fractions, and thus less resistance to the flow, the least pressure drop was observed during the big size particle tests.

Figure 4.13 illustrates the graphical deviation between experimentally and theoretically obtained pressure drops.
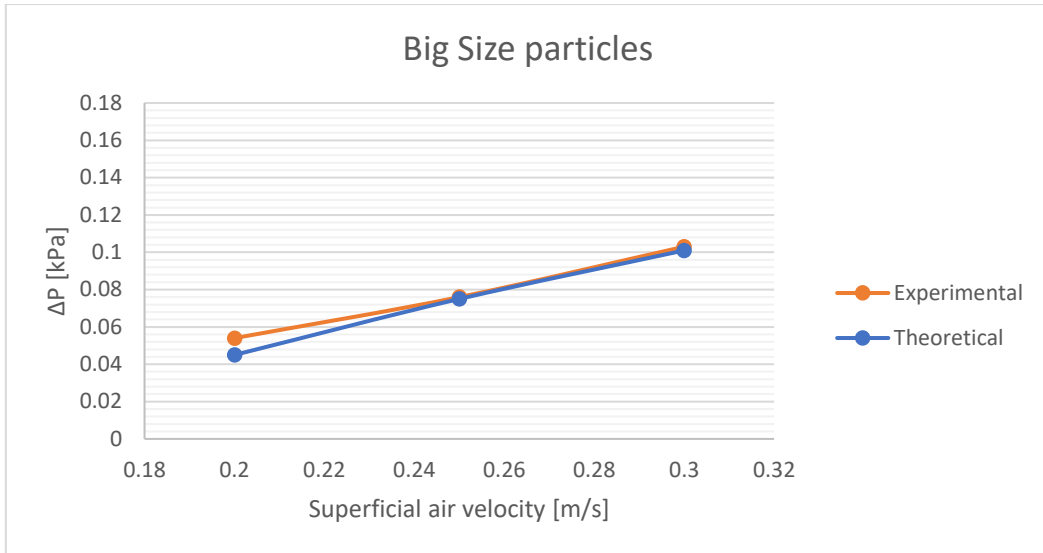
Figure 4.13: Pressure drop evaluation over big-size zeolite

5. Conclusion and Further Work

In this thesis, the CO_2 capture process by adsorption using zeolite adsorbents was studied. The theoretical background regarding the adsorption process, various CO_2 capture technologies, most prevalently used adsorbent materials, and present experimental researches have been covered. The principal goal of this thesis is to investigate how the Z8 test plant operates under different working conditions, to understand the effects of flowrate and adsorbent size on the adsorption capacity, and to suggest the improvements that the facility needs. As explained above in the 'Desorption Challenges' section, some hardships took place during the experimental procedure, which lingered the test period. However, the followings are the conclusions that can be made from this experiment:

1) As the flowrate increases, the breakthrough is observed in a shorter time
2) Till the breakthrough, external diffusion is dominant, and thus, the small size adsorbent is the slowest due to more active sites on the surface area.
3) From the breakthrough till the completion of the test, internal diffusion becomes dominant. And as the particle size increases, it becomes more difficult for adsorbent media to be fully saturated with CO_2.
4) Small size zeolite is the best considering its adsorption capacity, but not favorable regarding adsorption rate.
5) Medium size zeolite is the best in respect of capture rate but more prone to be disturbed by the flow at higher flowrates.
6) The higher the flowrate, the more adsorbed amount of CO_2 is observed from breakthrough until equilibrium.
7) According to both theory and experimental data, the bigger the particle size, the less pressure drop is observed.

The followings are the suggestions for the improvement of the test plant and further work.

- The pressure adjuster was not the best choice to decrease the compressed air pressure from 8 atm. down to atmospheric pressure. It consistently created difficulties such as fluctuating flowrate, and therefore, physical supervision until the end of the test was highly indispensable.
- The sensor of the Z8 facility for measuring the CO_2 concentration was not reliable, and consequently, the use of a Kimo measurement device was needed.
- The test plant needs better isolation to run the desorption process.

- More experiments should be implemented to get the optimum working conditions and thus increase the adsorption capacity of the adsorbents. One suggestion is to commence with a lower flowrate until breakthrough and shift to a higher flowrate from breakthrough until equilibrium adsorption.

References

[1]   'Global Emissions', *Center for Climate and Energy Solutions*, Jan. 06, 2020. https://www.c2es.org/content/international-emissions/ (accessed Apr. 08, 2021).

[2]   T. Eggleton and R. A. Eggleton, *A Short Introduction to Climate Change*. Cambridge University Press, 2013.

[3]   D. G. Kaufman, *Biosphere 2000 : protecting our global environment*. Dubuque, Iowa : Kendall/Hunt Pub. Co., 1996. Accessed: Jan. 18, 2021. [Online]. Available: http://archive.org/details/biosphere2000pro0000kauf

[4]   U.S. Global Change Research Program, Ed., *Global climate change impacts in the United States: a state of knowledge report*. Cambridge [England] ; New York: Cambridge University Press, 2009.

[5]   S. Topham *et al.*, 'Carbon Dioxide', 2014, pp. 1–43. doi: 10.1002/14356007.a05_165.pub2.

[6]   P. Freund, S. Bachu, D. Simbeck, and M. Gupta, 'Properties of CO2 and carbon-based fuels', p. 18.

[7]   R. Kusumastuti, Sriyono, M. Pancoko, S. L. Butar-Butar, G. E. Putra, and H. Tjahjono, 'Study On The Mechanism of CO $_2$ Adsorption Process on zeolite 5A as a Molecular Sieve In RDE System: An Infrared Investigation', *J. Phys. Conf. Ser.*, vol. 1198, no. 3, p. 032009, Apr. 2019, doi: 10.1088/1742-6596/1198/3/032009.

[8]   H. Hu and K. Xu, 'Chapter 8 - Physicochemical technologies for HRPs and risk control', in *High-Risk Pollutants in Wastewater*, H. Ren and X. Zhang, Eds. Elsevier, 2020, pp. 169–207. doi: 10.1016/B978-0-12-816448-8.00008-3.

[9]   N. Fouladi, M. A. Makarem, M. A. Sedghamiz, and H. R. Rahimpour, 'Chapter 11 - CO2 adsorption by swing technologies and challenges on industrialization', in *Advances in Carbon Capture*, M. R. Rahimpour, M. Farsi, and M. A. Makarem, Eds. Woodhead Publishing, 2020, pp. 241–267. doi: 10.1016/B978-0-12-819657-1.00011-6.

[10]   M.-W. Yang, N. Chen, C. Huang, Y. Shen, H. Yang, and C. Chou, 'Temperature Swing Adsorption Process for CO2 Capture Using Polyaniline Solid Sorbent', *Energy Procedia*, vol. 63, pp. 2351–2358, Dec. 2014, doi: 10.1016/j.egypro.2014.11.256.

[11]   A. Ntiamoah, J. Ling, P. Xiao, P. A. Webley, and Y. Zhai, 'CO2 Capture by Temperature Swing Adsorption: Use of Hot CO2-Rich Gas for Regeneration', *Ind. Eng. Chem. Res.*, vol. 55, no. 3, pp. 703–713, Jan. 2016, doi: 10.1021/acs.iecr.5b01384.

[12]   L. Rosa, D. L. Sanchez, G. Realmonte, D. Baldocchi, and P. D'Odorico, 'The water footprint of carbon capture and storage technologies', *Renew. Sustain. Energy Rev.*, p. 110511, Oct. 2020, doi: 10.1016/j.rser.2020.110511.

[13]   T. Wilberforce, A. G. Olabi, E. T. Sayed, K. Elsaid, and M. A. Abdelkareem, 'Progress in carbon capture technologies', *Sci. Total Environ.*, p. 143203, Nov. 2020, doi: 10.1016/j.scitotenv.2020.143203.

[14]   S. Pandey, S. Gupta, A. Tomar, and A. Kumar, 'POST COMBUSTION CARBON CAPTURE TECHNOLOGY', Nov. 2010.

[15]   A. S. Lee, J. C. Eslick, D. C. Miller, and J. R. Kitchin, 'Comparisons of amine solvents for post-combustion CO2 capture: A multi-objective analysis approach', *Int. J. Greenh. Gas Control*, vol. 18, pp. 68–74, Oct. 2013, doi: 10.1016/j.ijggc.2013.06.020.

[16]   M. Wang, A. Lawal, P. Stephenson, J. Sidders, and C. Ramshaw, 'Post-combustion CO2 capture with chemical absorption: A state-of-the-art review', *Chem. Eng. Res. Des.*, vol. 89, no. 9, pp. 1609–1624, Sep. 2011, doi: 10.1016/j.cherd.2010.11.005.

[17]   S. M. Carpenter and H. A. Long, '13 - Integration of carbon capture in IGCC systems', in *Integrated Gasification Combined Cycle (IGCC) Technologies*, T. Wang and G. Stiegel, Eds. Woodhead Publishing, 2017, pp. 445–463. doi: 10.1016/B978-0-08-100167-7.00036-6.

[18]   M. Kanniche, R. Gros-Bonnivard, P. Jaud, J. Valle-Marcos, J.-M. Amann, and C. Bouallou, 'Pre-combustion, Post-combustion and Oxy-combustion in thermal power plant for CO capture', *Appl. Therm. Eng.*, vol. 30, no. 1, p. 53, Oct. 2009, doi: 10.1016/j.applthermaleng.2009.05.005.

[19]   W. L. Theo, J. S. Lim, H. Hashim, A. A. Mustaffa, and W. S. Ho, 'Review of pre-combustion capture and ionic liquid in carbon capture and storage', *Appl. Energy*, vol. 183, pp. 1633–1663, Dec. 2016, doi: 10.1016/j.apenergy.2016.09.103.

[20]   B. G. Miller, '13 - Carbon Dioxide Emissions Reduction and Storage', in *Clean Coal Engineering Technology (Second Edition)*, B. G. Miller, Ed. Butterworth-Heinemann, 2017, pp. 609–668. doi: 10.1016/B978-0-12-811365-3.00013-2.

[21]   S. M. Carpenter and H. A. Long, '13 - Integration of carbon capture in IGCC systems', in *Integrated Gasification Combined Cycle (IGCC) Technologies*, T. Wang and G. Stiegel, Eds. Woodhead Publishing, 2017, pp. 445–463. doi: 10.1016/B978-0-08-100167-7.00036-6.

[22]   L. Zheng, '1 - Overview of oxy-fuel combustion technology for carbon dioxide (CO2) capture', in *Oxy-Fuel Combustion for Power Generation and Carbon Dioxide (CO2) Capture*, L. Zheng, Ed. Woodhead Publishing, 2011, pp. 1–13. doi: 10.1533/9780857090980.1.

[23]   A. Gambhir and M. Tavoni, 'Direct Air Carbon Capture and Sequestration: How It Works and How It Could Contribute to Climate-Change Mitigation', *One Earth*, vol. 1, no. 4, pp. 405–409, Dec. 2019, doi: 10.1016/j.oneear.2019.11.006.

[24]   M. Fasihi, O. Efimova, and C. Breyer, 'Techno-economic assessment of CO2 direct air capture plants', *J. Clean. Prod.*, vol. 224, pp. 957–980, Jul. 2019, doi: 10.1016/j.jclepro.2019.03.086.

[25]   A. A. Okesola, A. A. Oyedeji, A. F. Abdulhamid, J. Olowo, B. E. Ayodele, and T. W. Alabi, 'Direct Air Capture: A Review of Carbon Dioxide Capture from the Air', *IOP Conf. Ser. Mater. Sci. Eng.*, vol. 413, p. 012077, Sep. 2018, doi: 10.1088/1757-899X/413/1/012077.

[26]   X. Shi *et al.*, 'Sorbents for the Direct Capture of CO_2 from Ambient Air', *Angew. Chem. Int. Ed.*, vol. 59, no. 18, pp. 6984–7006, 2020, doi: https://doi.org/10.1002/anie.201906756.

[27]   *Read 'Negative Emissions Technologies and Reliable Sequestration: A Research Agenda' at NAP.edu*. doi: 10.17226/25259.

[28]   K. S. Lackner, 'The thermodynamics of direct air capture of carbon dioxide', *Energy*, vol. 50, pp. 38–46, Feb. 2013, doi: 10.1016/j.energy.2012.09.012.

[29]   J.-R. Li *et al.*, 'Carbon dioxide capture-related gas adsorption and separation in metal-organic frameworks', *Coord. Chem. Rev.*, vol. 255, no. 15, pp. 1791–1823, Aug. 2011, doi: 10.1016/j.ccr.2011.02.012.

[30]   B. Sreenivasulu, I. Sreedhar, P. Suresh, and K. V. Raghavan, 'Development Trends in Porous Adsorbents for Carbon Capture', *Environ. Sci. Technol.*, vol. 49, no. 21, pp. 12641–12661, Nov. 2015, doi: 10.1021/acs.est.5b03149.

[31]   D. M. D'Alessandro, B. Smit, and J. R. Long, 'Carbon Dioxide Capture: Prospects for New Materials', *Angew. Chem. Int. Ed.*, vol. 49, no. 35, pp. 6058–6082, 2010, doi: https://doi.org/10.1002/anie.201000431.

[32]   T. Khandaker, M. S. Hossain, P. K. Dhar, M. S. Rahman, M. A. Hossain, and M. B. Ahmed, 'Efficacies of Carbon-Based Adsorbents for Carbon Dioxide Capture', *Processes*, vol. 8, no. 6, Art. no. 6, Jun. 2020, doi: 10.3390/pr8060654.

[33]   M. Pardakhti *et al.*, 'Trends in Solid Adsorbent Materials Development for CO_2 Capture', *ACS Appl. Mater. Interfaces*, vol. 11, no. 38, pp. 34533–34559, Sep. 2019, doi: 10.1021/acsami.9b08487.

[34]   S. Choi, J. H. Drese, and C. W. Jones, 'Adsorbent Materials for Carbon Dioxide Capture from Large Anthropogenic Point Sources', *ChemSusChem*, vol. 2, no. 9, pp. 796–854, 2009, doi: https://doi.org/10.1002/cssc.200900036.

[35]   I. Markovska, 'SYNTHETIC ZEOLITES - STRUCTURE, CLASIFICATION, CURRENT TRENDS IN ZEOLITE SYNTHESIS REVIEW', Sep. 2009.

[36]   K. Ramesh and D. D. Reddy, 'Chapter Four - Zeolites and Their Potential Uses in Agriculture', in *Advances in Agronomy*, vol. 113, D. L. Sparks, Ed. Academic Press, 2011, pp. 219–241. doi: 10.1016/B978-0-12-386473-4.00004-X.

[37]   S. Kumar, R. Srivastava, and J. Koh, 'Utilization of zeolites as CO_2 capturing agents: Advances and future perspectives', *J. CO2 Util.*, vol. 41, p. 101251, Oct. 2020, doi: 10.1016/j.jcou.2020.101251.

[38]   M. Król, 'Natural vs. Synthetic Zeolites', *Crystals*, vol. 10, no. 7, Art. no. 7, Jul. 2020, doi: 10.3390/cryst10070622.

[39]   'Zeolite Molecular Sieves: Structure, Chemistry, and Use D. W. Breck (Union Carbide Corporation, Tarrytown, New York) John Wiley and Sons, New York, London, Sydney, and Toronto. 1974. 771 pp. $11.95', *J. Chromatogr. Sci.*, vol. 13, no. 4, pp. 18A-18A, Apr. 1975, doi: 10.1093/chromsci/13.4.18A-c.

[40]   A. Yu. Khodakov and L. V. C. Rees, 'Effect of propane on the kinetics of carbon dioxide adsorption in NaA zeolites', *Gas Sep. Purif.*, vol. 9, no. 4, pp. 253–257, Dec. 1995, doi: 10.1016/0950-4214(95)00007-X.

[41]   R. Hernández-Huesca, L. Díaz, and G. Aguilar-Armenta, 'Adsorption equilibria and kinetics of CO2, CH4 and N2 in natural zeolites', *Sep. Purif. Technol.*, vol. 15, no. 2, pp. 163–173, Mar. 1999, doi: 10.1016/S1383-5866(98)00094-X.

[42]   L.-Z. Zhang, H.-X. Fu, Q.-R. Yang, and J.-C. Xu, 'Performance comparisons of honeycomb-type adsorbent beds (wheels) for air dehumidification with various desiccant wall materials', *Energy*, vol. 65, pp. 430–440, Feb. 2014, doi: 10.1016/j.energy.2013.11.042.

[43]   A. Alahmer, S. Alsaqoor, and G. Borowski, 'Effect of parameters on moisture removal capacity in the desiccant cooling systems', *Case Stud. Therm. Eng.*, vol. 13, p. 100364, Mar. 2019, doi: 10.1016/j.csite.2018.11.015.

[44]   R. Pesic, T. Kaluđerović Radoičić, N. Boskovic-Vragolovic, Z. Arsenijević, and Z. Grbavcic, 'Pressure drop in packed beds of spherical particles at ambient and elevated air temperatures', *Chem. Ind. Chem. Eng. Q.*, vol. 21, pp. 419–427, Jul. 2015, doi: 10.2298/CICEQ140618044P.

[45]   A. G. Dixon, 'Correlations for wall and particle shape effects on fixed bed bulk voidage', *Can. J. Chem. Eng.*, vol. 66, no. 5, pp. 705–708, 1988, doi: https://doi.org/10.1002/cjce.5450660501.
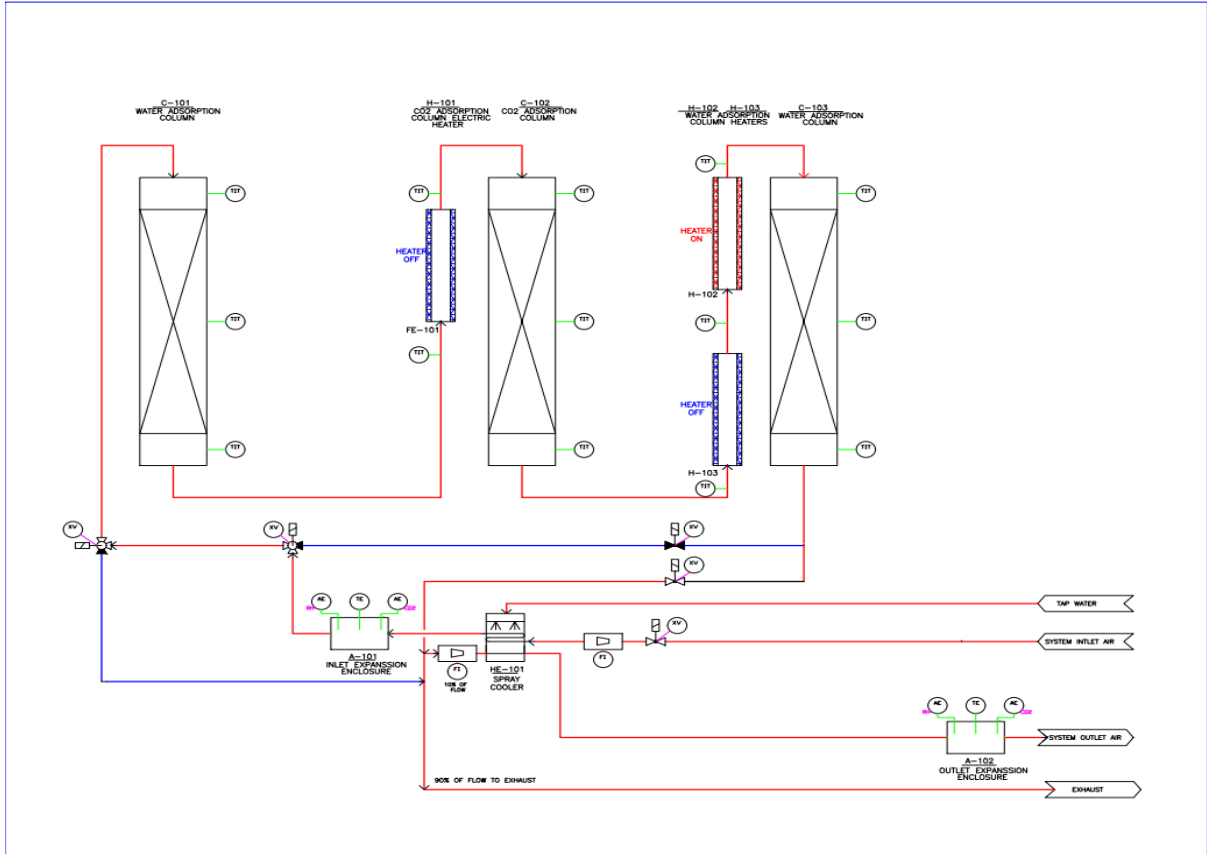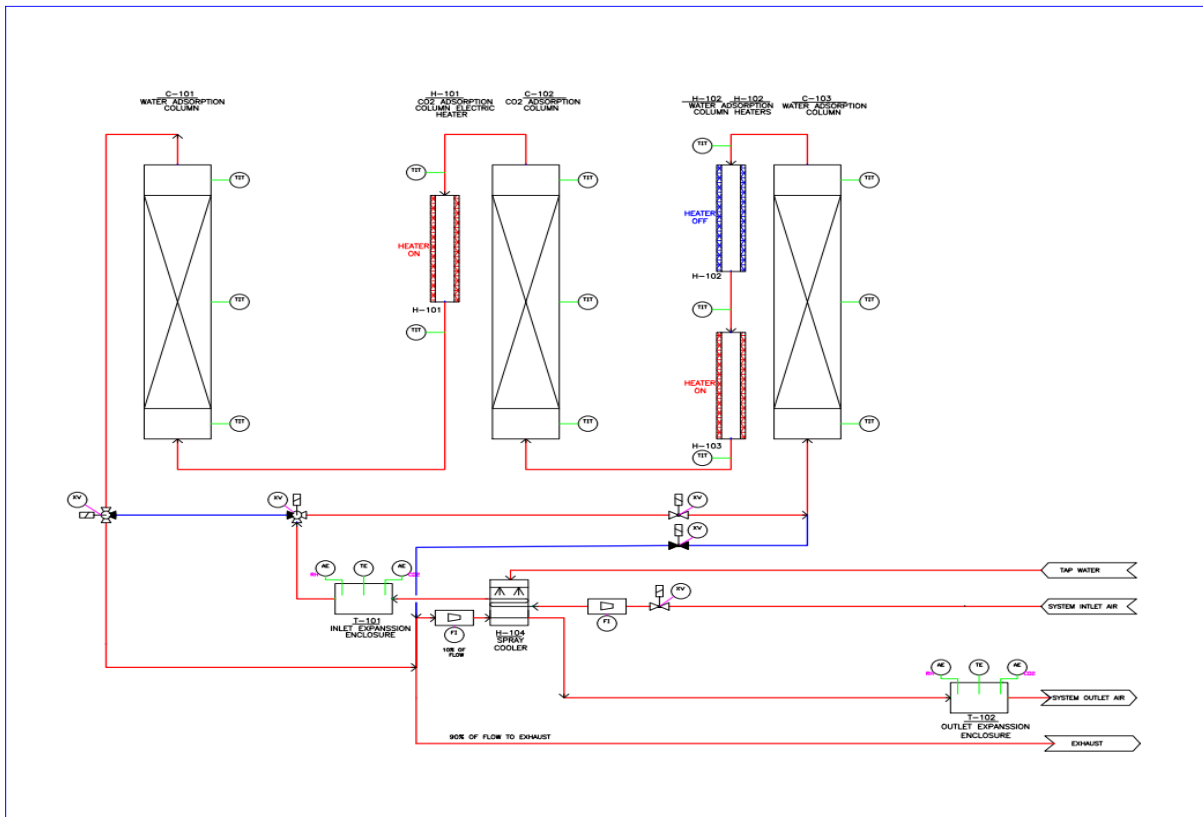
Appendix

A. P&ID of the test plant
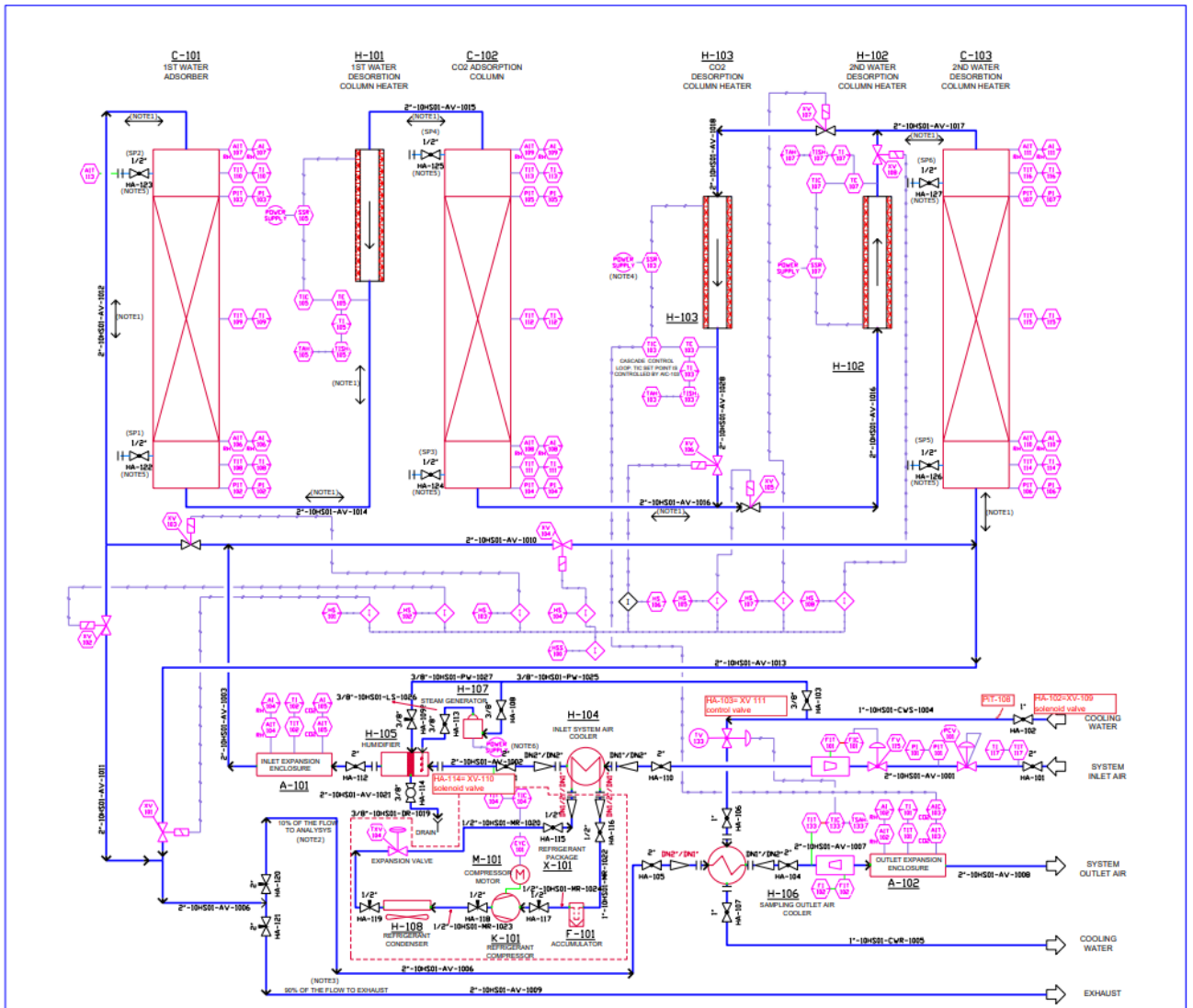
B. Process flow diagrams of the adsorption and desorption processes

Adsorption

Desorption

C. Datasheet of the test materials (provided by Greencap Solutions)

Small-size zeolite 13X

SYLOBEAD® MS C 544

Adsorbent for Drying and Purification of Gases and Liquids

Product Description

SYLOBEAD® MS C 544 Adsorbent for Drying and Purification of Gases and Liquids is a highly porous, crystalline aluminosilicate in beaded form. The pore openings in the crystals have a diameter of approximately 10 Å.

Typical Properties and Recommended Applications

The following typical properties data are given for informational purposes only, and are not to be interpreted as product or in-process specifications.

Property	UOM	Value
Bulk Density	g/l	675
Total Volatile (950°C)	%	2.0
Residual Water Content (LOI, 575°C)	%	1.5
H_2O-Adsorption Capacity 10% r.h., 25°C	%	23.0
H_2O-Adsorption Capacity 80% r.h., 25°C	%	29.0
CO_2-Adsorption Capacity 2 torr, 25°C	%	5.0
CO_2-Adsorption Capacity 250 torr, 25°C	%	19.0
H_2S-Adsorption Capacity, 5 torr, 25°C	%	11.0
Crush Strength	N	40
Bead Size	mm	1.6 – 2.5

SYLOBEAD® MS C 544 Adsorbent for Drying and Purification of Gases and Liquids adsorbs molecules with effective diameters smaller than approximately 10 Å. Due to its high capacity for water and CO_2 this molecular sieve is widely used for air purification in cryogenic air separation plants. It is also applied in the removal of H_2S/mercaptans and other sulphur compounds from natural gas and LPG.

Packaging Information

The standard packaging for SYLOBEAD® MS C 544 Adsorbent for Drying and Purification of Gases and Liquids is:

130 kg/drum	4 drums/pallet	520 kg/pallet	pallet: 1200 x 1000 mm
800 kg/big bag	1 bag/pallet	800 kg/pallet	pallet: 1200 x 1000 mm

Medium-size zeolite 13X

SYLOBEAD® MS C 542

Adsorbent for Drying and Purification of Gases and Liquids

Product Description

SYLOBEAD® MS C 542 is a highly porous, crystalline aluminosilicate in beaded form. The pore openings in the crystals have a diameter of approximately 10 Å.

Typical Properties and Recommended Applications

The following typical properties data is given for informational purposes only and is not to be interpreted as product or in-process specifications.

Property	UOM	Value
Bulk Density	g/l	640
Total Volatile (950°C)	%	2.0
Residual Water Content (LOI, 575°C)	%	1.5
H_2O-Adsorption Capacity 10% r.h., 25°C	%	23.0
H_2O-Adsorption Capacity 80% r.h., 25°C	%	29.0
CO_2-Adsorption Capacity 2 torr, 25°C	%	5.0
CO_2-Adsorption Capacity 250 torr, 25°C	%	19.0
H_2S-Adsorption Capacity, 5 torr, 25°C	%	11.0
Crush Strength	N	80
Bead Size	mm	2.5 – 5.0

SYLOBEAD® MS C 542 Adsorbent for Drying and Purification of Gases and Liquids adsorbs molecules with effective diameters smaller than approximately 10 Å. Due to its high capacity for water and CO_2 this molecular sieve is widely used for air purification in cryogenic air separation plants. It is also applied in the removal of H_2S/mercaptans and other sulphur compounds from natural gas and LPG.

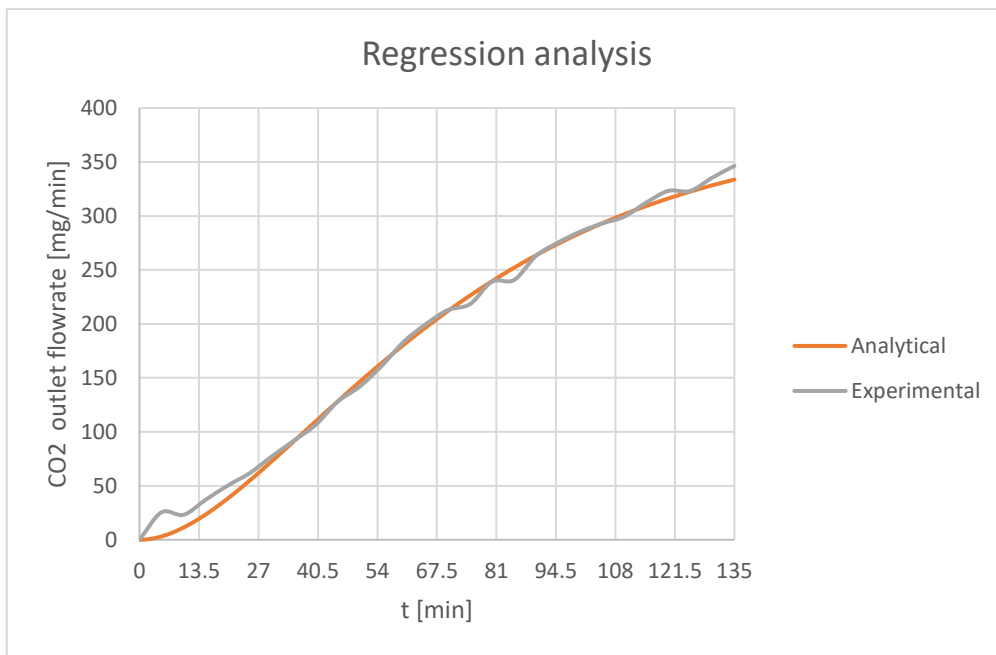## D. Plots from the rest regression tests

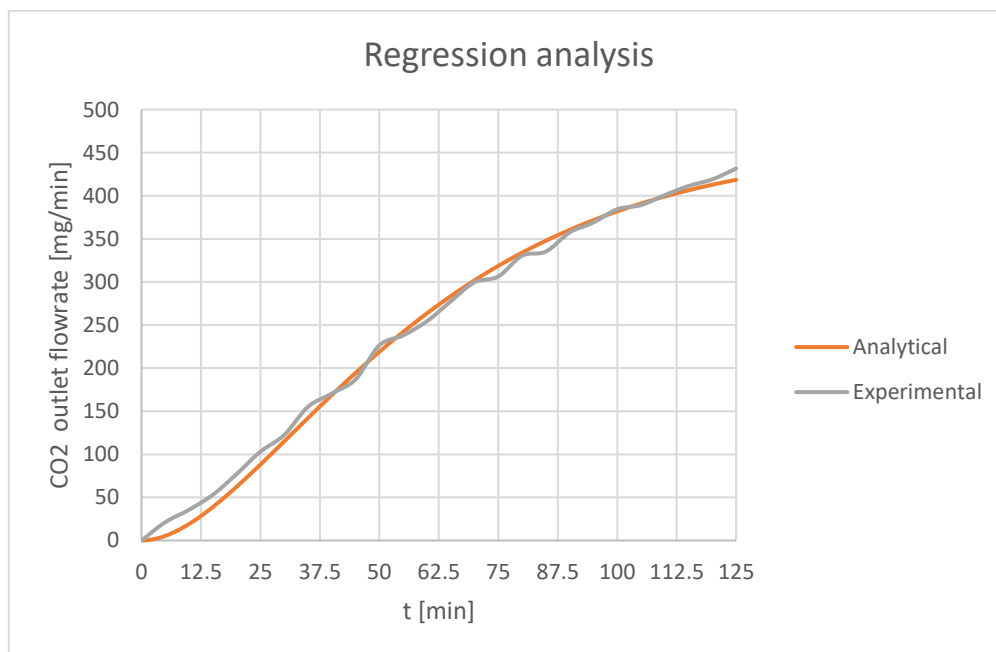Figure 5.1: Test 1.1 Small-size zeolite 13X

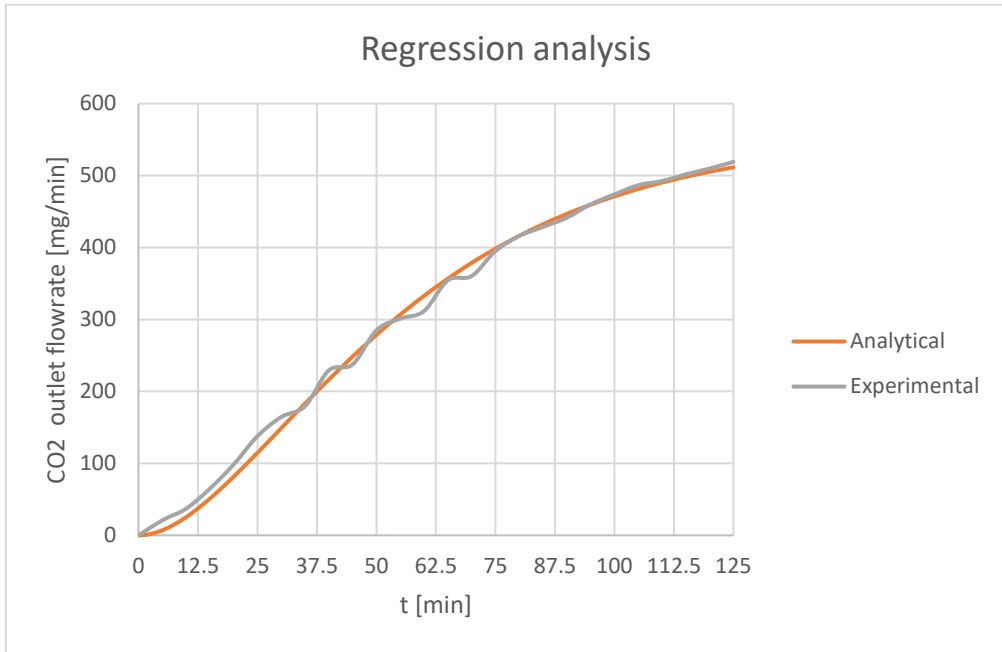Figure 5.2: Test 1.2 Small-size zeolite 13X

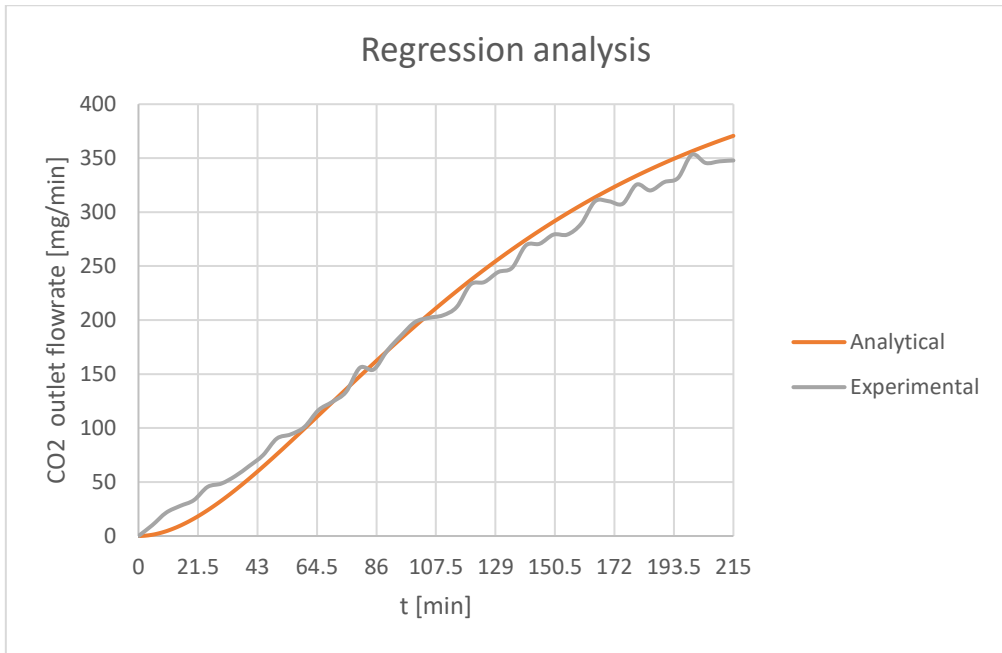Figure 5.3: Test 1.3 Small-size zeolite 13X

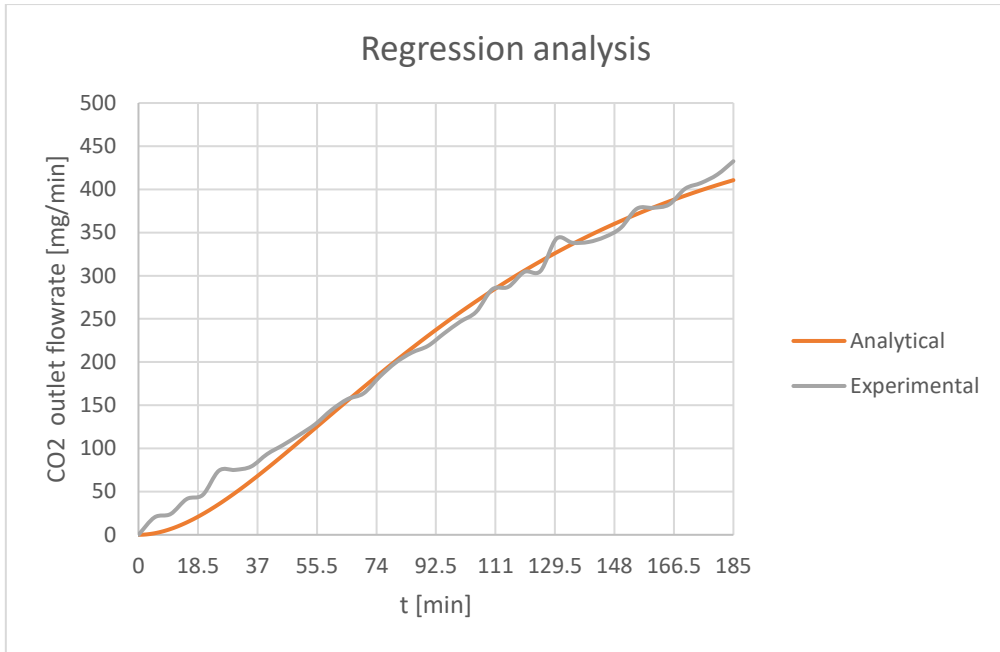Figure 5.4: Test 1.4 Medium-size zeolite 13X

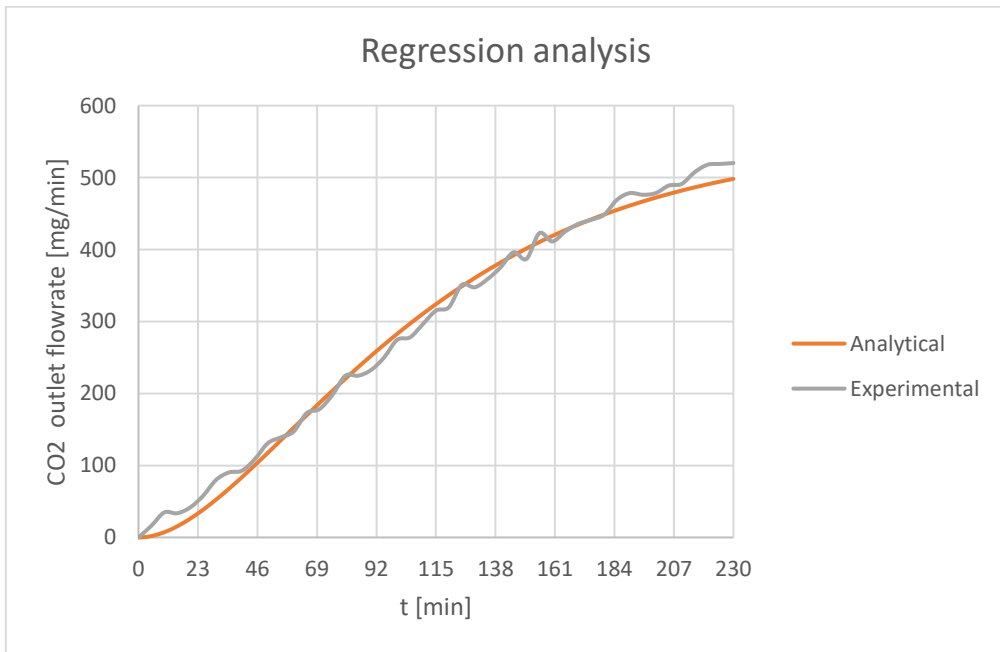Figure 5.5: Test 1.5 Medium-size zeolite 13X
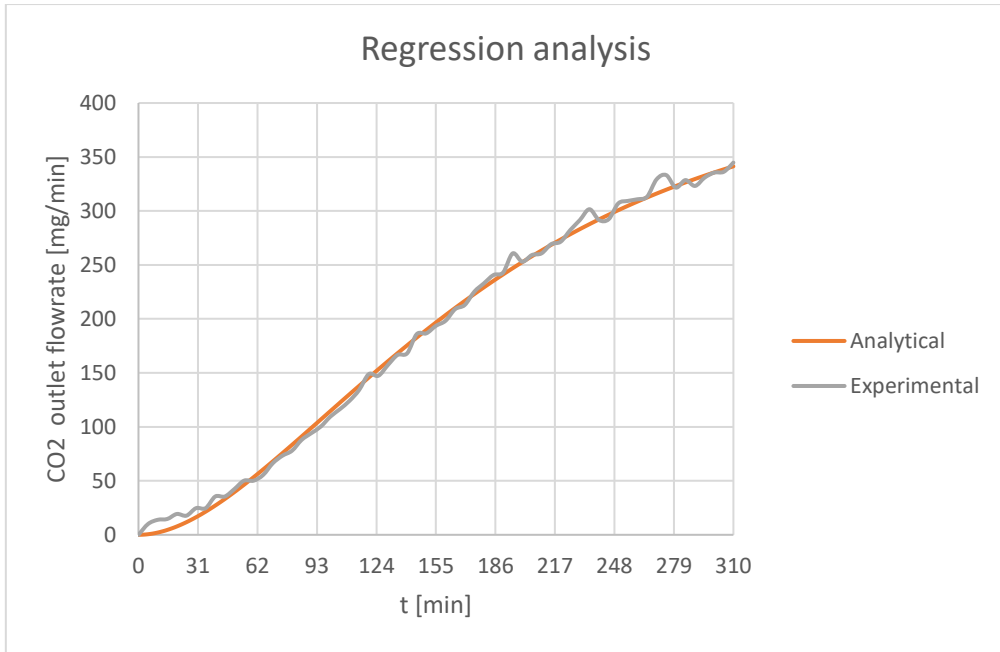

Figure 5.6: Test 1.6 Medium-size zeolite 13X
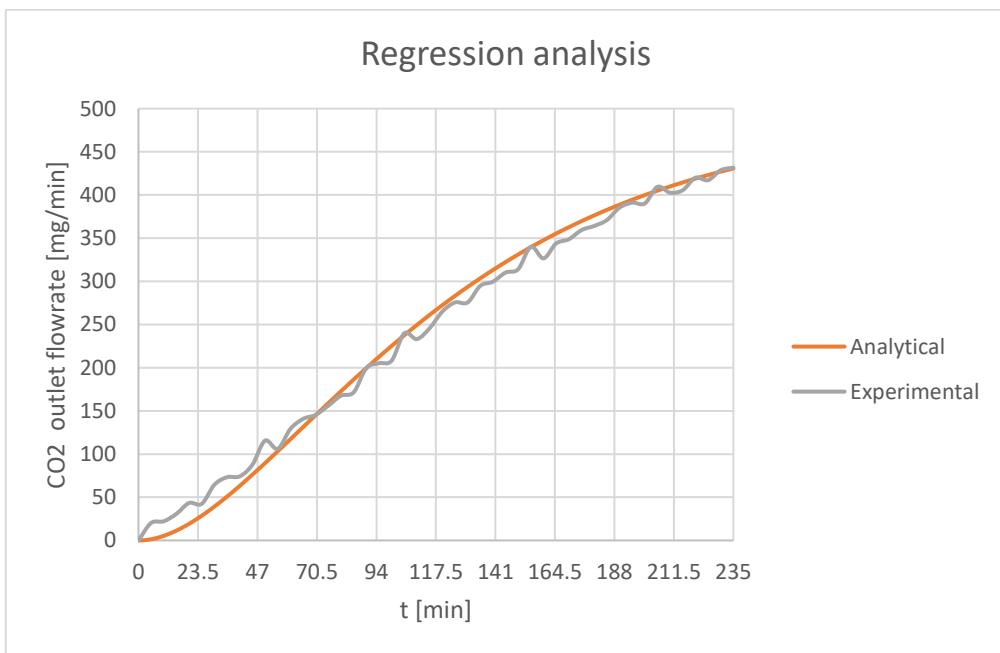
Figure 5.7: Test 1.7 Big-size zeolite 13X

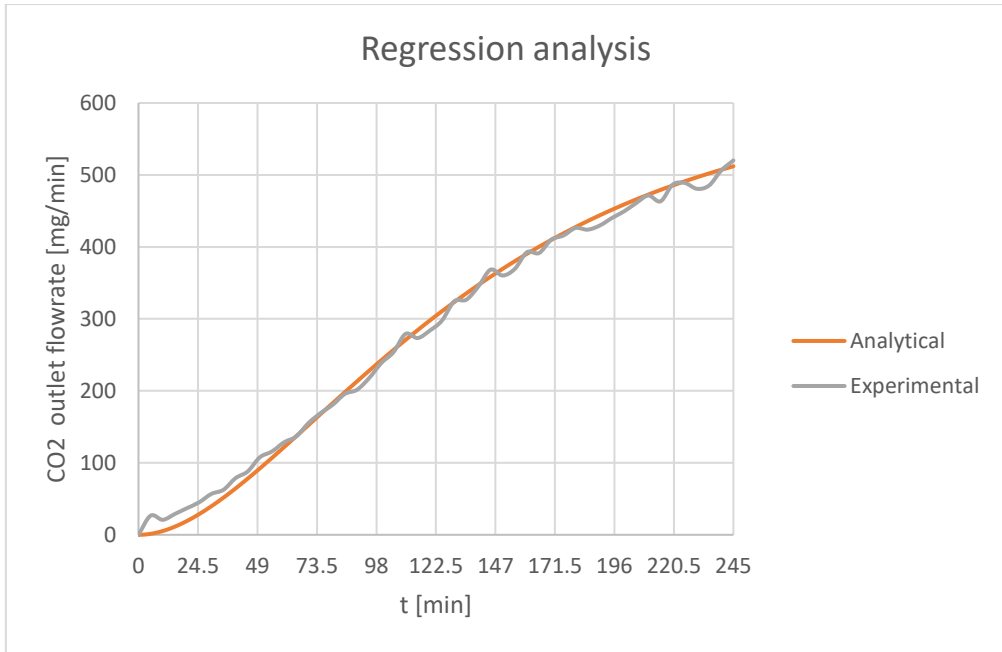Figure 5.8: Test 1.8 Big-size zeolite 13X

Figure 5.9: Test 1.9 Big-size zeolite 13X

E. Visual illustrations of the test plant